AIR FORCE INSTITUTE OF TECHNOLOGY

AIR UNIVERSITY
UNITED STATES AIR FORCE

Oxidation of Rene 41 and Thoriated Nickel Wires
Between 1600 F and 2000 F

by

Robert A. Rosenberg

Capt   USAF

Mech/GAW 18-64

SCHOOL OF ENGINEERING

WRIGHT-PATTERSON AIR FORCE BASE, OHIO

Best
Available
Copy

Oxidation of Rene 41 and Thoriated Nickel Wires
Between 1600 F and 2000 F

by
Robert A. Rosenberg

Capt   USAF

Mech/GAW 18-64

OXIDATION OF RENE 41 AND THORIATED NICKEL WIRES

BETWEEN 1600 F AND 2000 F

THESIS

Presented to the Faculty of the School of Engineering of

the Air Force Institute of Technology

Air University

in Partial Fulfillment of the

Requirements for the Degree of

Master of Science

By

Robert Alan Rosenberg, B. S. General Engineering

Capt   USAF

Graduate Air Weapons

June 1964

Preface

The purpose of this investigation was to examine and evaluate the high-temperature oxidation characteristics of two high-strength nickel-base alloys, Rene 41 and Thoriated Nickel, under a variety of test parameters which included time, temperature, geometry, stresses and oxygen partial pressures. Wire specimens were selected for examination because of the many potential applications for their use, such as expandable structure and re-entry drag chute materials and heater elements.

The evaluation of the oxidation kinetics of Rene 41 wire was particularly interesting, in that the theoretical literature from which I derived my background discussed only the oxidation characteristics of simple systems. Rene 41, which is composed of 12 elements, most certainly would be expected to deviate from the ideal!

I wish to express my appreciation to Dr. S. T. Wlodek of the General Electric Materials Development Laboratory, Cincinnati, for his invaluable advice and assistance in interpretation of test results. I want to thank my advisor, Dr. Richard K. Saxer, and Professor James Myers for their aid, interest, and enthusiasm during the long hours of testing. Finally, I am deeply indebted to Mr. Paul Faust of the Materials Testing Laboratory, Wright-Patterson AFB, for his help with regard to oxidation testing and theory and for his assistance in the area of logistics support.

Contents

Contents

List of Figures

List of Figures

Abstract

Oxidation rates of 10 and 20 mil nickel-base superalloy wires, Rene 41 and Thoriated Nickel, were measured over the range 1600 F to 2000 F for up to 1000 minutes using gravimetric methods. Rene 41 wire oxidation was characterized by the rapid growth of Al_2O_3 caused by a high concentration gradient of aluminum. Formation of this protective Al_2O_3 scale resulted in much slower oxidation of chromium from the normal parabolic rates observed for 50 mil Rene 41 sheet. A theoretical analysis based on diffusion theory for cylindrical shapes was presented to explain the measured oxidation rates. TD Nickel oxidation exhibited a parabolic rate of reaction, controlled by the growth of NiO. Both alloys suffered increases in oxidation rates with increases in temperature.

Oxidation of Rene 41 wire increased with the application of stress, while TD Nickel oxidation was insensitive to stress. Internal oxidation (Al_2O_3) of Rene 41 occurred, whereas the high density surface scale of TD Nickel and lack of alloys within its matrix prevented internal oxidation. Neither alloy appeared sensitive to a decrease in O_2 partial pressure.

BLANK PAGE

OXIDATION OF RENE 41 AND THORIATED NICKEL WIRES
BETWEEN 1600 F and 2000 F

I. Introduction

The Problem

High-Temperature Oxidation. The purpose of this investigation was
to determine the effects of several test variables on the oxidation of
superalloy wires. The variables considered in this experiment included
time, temperature, geometry, stress, oxygen partial pressure, and ther-
mal cycling.

Scope. Because the overall problem of evaluating the oxidation
characteristics of superalloys was too broad a field for examination,
the wires selected represented two of the most suitable alloys for
aerospace applications; the selection being made from evaluation of
mechanical properties determined by other investigators (See Appendix
C).

No attempt was made to evaluate creep, stress-rupture, or other
mechanical and physical phenomena quantitatively in this experiment.
These items were generally observed for satisfactory comparison with
previously established properties.

Concepts and Definitions. The wire materials selected, Rene 41
and Thoriated (TD) Nickel, were subjected to the testing environment
under least favorable conditions, by oxidizing unprotected samples.
An unprotected sample refers to a specimen having no corrosion-resistant
coating for protection from adverse environmental conditions. Testing
this type of specimen permitted more thorough analysis of the surface
and internal oxidation characteristics of the wire.

Superalloys are metal compounds with a base of iron, nickel, or
cobalt. Relatively high strength-to-weight ratio, ductility, and good
oxidation resistance in the temperature range from 1400 F to 2200 F are
the most important qualities found in these alloys. TD Nickel and

Rene 41, both nickel-base superalloys, exhibit above-average high-temperature properties. Most practical applications for superalloys include high-temperature environments, thermal cycling and stress, changes in oxygen pressure, and different exposure times. Therefore, test variables were imposed to examine any anomalies from normal atmosphere corrosion; better simulating anticipated aerospace environments.

Historical Review

With the advent of the space age, new materials for adaption to the peculiar environmental conditions encountered in space had to be developed. The use of metal filaments had been considered for fabrication of expandable structure materials and tank skins (Ref 19:768; 9:47). One particular new concept, the deceleration of a re-entry vehicle by drag-chute techniques (Ref 45), required the selection of suitable metal filaments, or wires, for use in weaving metal parachutes. The metal to be selected had to exhibit high strength and ductility, ease of fabrication, and good oxidation resistance.

The Aeronautical Systems Division, USAF, conducted a survey study in 1962 to determine what metals could best meet operational criteria for high-temperature fabrics. Refractories and ceramics, although both capable of withstanding very high stresses, were extremely brittle. Steel alloys, although ductile, became weak at anticipated exposure temperatures. The superalloys were chosen as the most suitable candidates, and of several alloys tested, Rene 41 and TD Nickel exhibited above-average mechanical properties.

The previous experiments conducted to select suitable superalloys were concerned with mechanical properties, the one exception being Johnson, et al (Ref 22), who measured 10 minute oxidation rates for superalloy wires. This author, therefore, determined that a study of the oxidation of Rene 41 and TD Nickel wires would be a contribution to the literature on high-temperature superalloys.

Summary of Results

The oxidation studies conducted on Rene 41 and TD Nickel 10 and 20 mil wires revealed significant characteristics of the two metals upon exposure to a high-temperature environment. Rene 41 wires oxidized more rapidly on initial exposure to temperature than thick sheet material. The larger diameter wire suffered the most oxidation initially; however, as exposure was continued, 20 mil wire oxidized at the slowest rate, because of the initial, rapid build-up of a protective Al_2O_3 coat. The reaction in both wire and sheet were expressed mathematically as

$$\Delta m^b = kt \qquad (1)$$

where Δm is weight change per unit area, b is an experimentally determined constant, k is the rate constant, and t is time. The exponent, b, was 2 for the sheet material, resulting from parabolic kinetics. b ranged from 2.3 to 3 for 10 mil wire and ranged from 4 to 8.5 for 20 mil wire, depending on temperature. These exponents indicated that 20 mil wire continued to oxidize at a slower overall rate than 10 mil wire or sheet.

Test results showed that Rene 41 oxidation was increased by the application of stress, and that internal oxidation occurred after prolonged exposure times (200 minutes).

TD Nickel wire exhibited parabolic oxidation kinetics, with the resultant formation of a tenacious oxide, NiO, on the surface. No internal oxidation or effect of stress on oxidation of TD Nickel were noted in the experiment. Both Rene 41 and TD Nickel oxidation rates appeared insensitive to a reduction in O_2 partial pressure to $5‰$, primarily because diffusion of metal ions, rather than oxygen, was the rate controlling process.

The oxide formed on Rene 41 spalled at weight gains in excess of 1.5 to 2 mg/cm^2 in 20 mil wire. TD Nickel scale was much more adherent, with no spalling occurring throughout the test cycle.

II. Background Investigation

Rene 41

Historical Development. One of the earliest references to nickel-chrome alloys was a 1906 British patent stating that Ni-Cr alloys of less than 25‰ chromium displayed excellent oxidation resistance at high temperatures. Later, British research revealed that as the chromium content was increased from 20‰ to 30‰, oxidation resistance was increased; however, above 750 F, creep rates also were accelerated. This knowledge resulted in the production of the first precipitation-hardened nickel-base superalloy, Nimonic 80 (Ref 20:2). Parallel studies in the U.S. in 1941 led to the development of Inconel X. During the latter part of World War II, a need for better high-temperature alloys was accentuated by the requirements of aerospace designers to fabricate sheet metal components for engine compressor and turbine frames (Ref 30:67). Complex heat treatments to obtain better mechanical properties, and variation of alloying element percentages to obtain optimum physical properties led to the development of the present superalloys, which satisfy many high-temperature aerospace requirements today (Ref 20:7-8).

Strengthening Mechanism. Currently, Rene 41 is one of the strongest Ni-Cr superalloys in production, attaining its high strength and hardness characteristics by precipitation hardening and solid-solution hardening. Strengthening effects are contributed by strain fields about alloying elements, impeding dislocation movement. Precipitation from solid solution of a second phase, $Ni_3(Al,Ti)$, with resultant internal strain fields also tends to impede dislocation movement (Ref 2:95). Unlike other nickel-base alloys which attain better stress-rupture life from carbide precipitation, carbides cause the formation of brittle grain-boundary networks in Rene 41 (Ref 2:99-103); therefore, they must be retained in solid solution to maintain desirable strengthening properties.

The strengthening process, called "precipitation hardening", involves heating of the base metal and alloying elements to a "solution" temperature of 1950 F to 2100 F, then quenching in air to retain the alloy in the base-metal crystalline structure. Aging of the solid solution at elevated temperatures from 1450 F to 1750 F then develops alloy strength as the solute atoms begin to precipitate out of solution, creating high-energy strain fields. Maximum hardness occurs when the alloying elements are just barely coherent to the nickel lattice, thereby affecting a large portion of the lattice and maximizing resistance to the movement of dislocations (Ref 18:445-447; 2:96-97). An attractive feature of Rene 41 is its extreme resistance to overaging, the main concern of precipitation-hardening alloys (Ref 2:95). This resistance is caused by the high stability of the intermetallic compound, $Ni_3(Al,Ti)$.

Effects of Alloying Elements on Rene 41. Chromium improves oxidation resistance and solid-solution strength up to approximately 30%, but additional amounts above 20% tend to decrease creep resistance. Cobalt, with an atomic radius approximately the same as nickel, forms a substitutional-solid solution in Rene, increasing melting temperature limits. Variations in the composition of Ni, Fe, and Co control the effective tolerance of the alloy for impurities. For matrix strength, molybdenum is added, but must be held to low amounts to avoid brittle intermetallic phases and internal oxidation. Boron in very small amounts improves ductility. Titanium and aluminum both improve the strength of the alloy and are a requirement in age-hardening processes. Aluminum is effective in reducing oxidation through formation of a protective oxide (Ref 12:5-6).

Thoriated Nickel

Historical Development. TD Nickel is a relatively new alloy for high temperature (1600 F to 2400 F), high strength applications,

developed by Du Pont after seven years of research concerned with the characteristics of dispersion hardening of various metals. Historically, dispersion hardening has not been employed as a strengthening technique because of the problem of achieving uniform dispersion of second-phase particles. Finally, in 1962, Du Pont succeeded in producing a uniformly-dispersed second phase, thoria (ThO_2), in a high-purity nickel base.

Strengthening Mechanism. TD Nickel derives its strength from the uniform dispersion of ThO_2 in the nickel matrix, blocking grain boundary and dislocation movement in the same manner as precipitates do in Rene 41, but with the advantage that desirable mechanical properties are retained at temperatures well above the solution temperature of Rene 41 and other superalloys (Ref 44:3). The dispersion hardening process employed is patented by Du Pont and involves powder metallurgy preparation of nickel and ThO_2 by a codeposition process. The powder is compacted under high pressure and sintered, producing uniform dispersion of ThO_2 in the nickel matrix (Ref 27:2; 44:3).

The physical and mechanical properties of Rene 41 and TD Nickel are adequately described in the literature and will not be covered here. A bibliography of articles reviewed by this author concerning these properties is included in Appendix C.

High-Temperature Oxidation

Theory and Mechanisms. The reaction between a metal and oxygen is a very complex subject, complicated by the addition of alloying elements to the base metal. However, oxidation is actually a special case of chemical kinetics, therefore, an investigation of any such reaction may be evaluated by comparison with established theoretical chemical laws (Ref 33:93).

Reactions normally follow a sequence of steps, one or more of which may control the overall rate of reaction. These include, but are not

limited to, diffusion of metal within an alloy, adsorption of oxygen at the oxide-gas interface, ionization of metal and/or oxygen, diffusion of metal ions outward through the oxide, diffusion of oxygen inward through the oxide, reaction between metal and oxygen, diffusion of reaction products away from each other, and reaction of oxidation products with one another. When alternative combinations of these reactions lead to the same result, the faster route will be rate determining; however, in interdependent oxidation processes, the slowest mechanism will control the reaction rate.

When a metal is exposed to oxygen, the reactants go to products according to the equation:

$$\text{Metal} + O_2 \longrightarrow \text{Metal Oxide} + \text{Energy} \qquad (2)$$
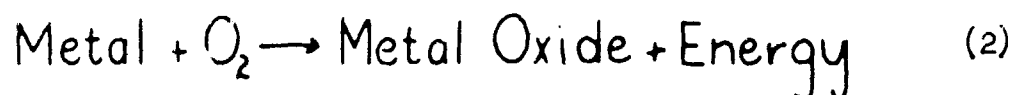
This results in a decrease in free energy for the system when the reaction proceeds from left to right as is the case for all but the most noble metals.

This reaction can be examined from an electrochemical viewpoint by realizing that oxidation (electron loss) occurs at the anode, and reduction (a gain of electrons) occurs at the cathode, as shown in Fig. 1. Oxidation rates then will be determined by the rate of production and flow of ions between the anodic and cathodic areas (Ref 4:17-23).

FIG. 1   OXIDATION AS AN ELECTROCHEMICAL PROCESS
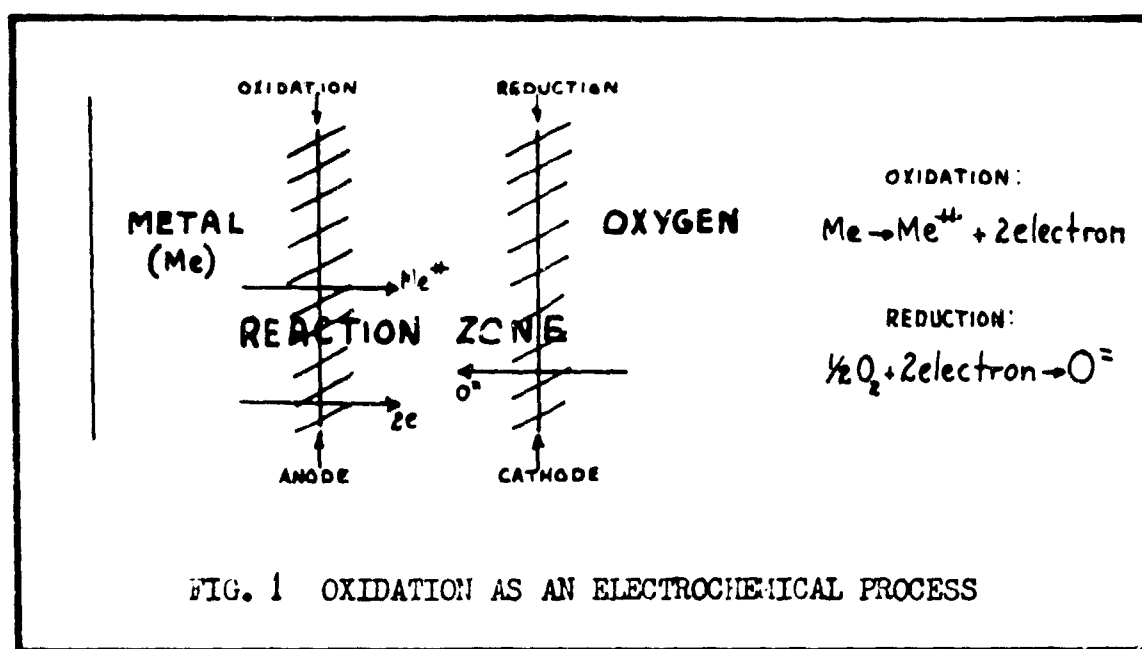
Being an electrical semi-conductor, oxide conductivity will depend on the relative concentrations of metal and oxygen as well as temperature (Ref 24:35-36). This results in the existance of two types of semi-conductor oxides, positive carriers and negative carriers. In the positive type, metal ion vacancies exist, requiring an equal number of electron vacancies for electrical neutrality. These vacancies form at the oxide-gas interface during oxidation and move to the metal surface. The negative-type oxide has an overbundancy of metal ions and electrons in the oxide lattice, and these migrate outward during oxidation to the oxide-gas interface (Ref 47:162). Impurities in the positive carrier may increase or decrease the number of electron vacancies for electrical equilibrium. This creates a corresponding decrease or increase in metal ion vacancies and a change in oxidation characteristics (Ref 47:163-164).

An excellent summary of the factors affecting oxidation has been written by Ignatov and Shamgunova as follows (Ref 21:4-5):

The rate of metal oxidation upon heating will be determined by the following factors: crystallochemical relationship between the metal and oxide lattices; parameters of the diffusion of metal or oxygen ions through the oxide film, depending upon the types of defects in the lattices of the oxides; phase and chemical transformations in the film (especially in multicomponent oxide films); and phase and other transformations in the metal itself.

Other factors also affect the rate of oxidation, such as: stresses arising in the scale; recrystallization processes in the film; the development of grains; and the physicochemical properties of the oxides (stability, volatility of the oxides, melting point, coefficient of expansion, porosity, plasticity, and mutual solubility of metal and oxide).

In case of alloys (especially multicomponent alloys), to those factors which affect the oxidation rate may be added the following: 1) thermodynamic activity of alloy components, which will be determined by the concentration of ions of the different components at the alloy-film boundary; 2) parameters of the diffusion of these components through the film; 3) secondary oxidation and reduction reactions in the film at the alloy-film boundary; 4) reactions between oxides of the different components in the film, of the type: $NiO + TiO_2 = NiTiO_3$; $NiO + Al_2O_3 = NiAl_2O_4$, etc., and 5) decomposition of complex oxide compounds at high temperatures, and vaporization of some of them.

Oxidation Rates. Although each metal has individual oxidation characteristics, general trends have been established empirically, and theoretically justified for a few specific oxidation rates. Some of the rates measured experimentally can be described by means of the following mathematical relationships:

$$\Delta m = k \log(at + c) \tag{3}$$

$$\Delta m = kt + c \tag{4}$$

$$\Delta m^2 = kt + c \tag{5}$$

$$\Delta m^b = kt + c \tag{6}$$

where Δm is the change in weight per unit area or the thickness of the oxide, a, b, and c, are experimentally determined constants, t is time, and k is a constant, referred to as the "rate constant". The constant, c in these equations represents the presence of an oxide coating on the metal at the beginning of an experiment. This film is usually quite small, and can be neglected in the determination of most rates (Ref 24:41).

An explanation of Eq (3) has been presented by Evans (Ref 10:135-138), wherein he postulates that compressional stress causes blisters to form as the oxide grows. Some of these blisters do not allow oxygen penetration through their surface nor metal ion movement outward. As oxidation proceeds, more of these impermeable scales form, causing the rate of oxidation to decrease exponentially. Further theoretical justification of the logarithmic rate has been stated by Mott and Cabrera (Ref 4:53-56) using an electrochemical approach involving the initial buildup of a thin film at low temperatures across which metal assumes a positive charge. At high temperatures, approaching oxygen molecules ionize and penetrate the thin film due to a potential difference. This results in migration of metal ions through the oxide. As the oxide film grows, the electric field influence is masked, resulting in an exponential decrease in rate.

Linear rates, Eq (4), occur when the oxide specific volume is smaller than that of the metal; resulting in spalling of the oxide and continual fresh exposure of the base metal to oxygen. If the scale does not exfoliate it will be relatively porous offering little resistance to oxygen penetration, and diffusion will be so rapid that concentration gradients can be neglected (Ref 43:312; 1:187). Wlodek (Ref 52:10-11) experimentally determined a linear rate for oxidation of Rene 41 and Udimet 700 at 1600 F to 2000 F in the early stages of attack; however, short time oxidation test data on Rene 41, Elgiloy, and Inconel 702 wires reported by Johnson, et al (Ref 23:6-14) were

fitted to a parabola.

A parabolic oxidation rate, Eq (5), was observed by Sartell and Li (Ref 41:92) in testing nickel at 1000 C. This observation was also reported by many other investigators who have tested 80‰-20‰ Ni-Cr alloys (Ref 14:163), Hastelloy X, Inconel 600, 702, and Nicrome 5 (Ref 46:339), Nickel (Ref 15:451; 16:128), Ni-Cr (Ref 14:163), and Rene 41 and Udimet 700 (Ref 52).* Mathematical analysis will show that diffusion processes are rate controlling (Ref 33:104) when parabolic rates are observed, and therefore, as the oxide thickness increases, more resistance to diffusion of oxygen and metal is provided (Ref 43:312; 10:142-7). A diffusion controlled process is one in which the flux, or amount of metal ions or oxygen ions passing at right angles through a unit area of reaction zone per unit time, is proportional to the concentration gradient of the diffusing ions. This has been expressed mathematically by Fick, who wrote

$$J = -D(\partial C/\partial X) \tag{7}$$

where J is flux, or rate of transfer per unit area, C the concentration, X the direction of diffusion, and D is a proportionality factor called the diffusion coefficient. By considering that the rate of growth of diffusing ions in a specified volume is the difference between the amount entering and leaving that volume, Fick concluded that

$$\partial C/\partial t = D(\partial^2 C/\partial X^2) \tag{8}$$

---

* Examination of the data in Refs 14, 15, 16, 41, 46, 52 by this author has led to the conclusion that in many cases, data points adhere more to a power series where the power is not an integer.

which is the fundamental differential equation of diffusion (Ref 7: 437-39).

The classical explanation of the parabolic rate was theorized by Wagner, who stated that concentration gradients within an oxide must exist in order for diffusion to occur, thus lattice imperfections will be present. Movement of the metal ions and electrons through such an oxide layer then determines the oxidation rate (Ref 24:120-130). Wagner's theory, which is based on Frenkel's mechanism of the electro-conductivity of oxide semi-conductors, is an application of the electro-chemical method of analyzing oxidation.

Power series rates, Eq (6), presently do not have strong theoretical backgrounds, but appear to be the results of combinations of one or more of the simpler theories, proceeding simultaneously (Ref 49: 4-25).

Deviations from the basic theories often occur, especially during the initial phases of oxidation, therefore, initial test data should be ignored when mathematically determining rates (Ref 43:313). Deviations later may occur for many reasons, including spalling, as Wlodek (Ref 52:25) found with Udimet 700, Hastelloy X and Rene 41 after prolonged exposure.

Normally, rate data is plotted as weight-gain per unit area versus time (Ref 33:94), although many authors prefer to plot parabolic rates as (weight-gain per unit area)^2 versus time. When power series data is plotted on log-log paper, it will lie along a straight line, the slope of which will represent the reciprocal of the power exponent. The rate constant, k, may then be calculated.

From the Arrhenius equation

$$k = A e^{-Q/RT} \qquad (9)$$

where A is a constant, R the gas constant, T the absolute tempera-
ture, and Q the activation energy of the reaction (Ref 24:46-47), Q
may sometimes be determined from the slope of the line plotted for
values of log K versus $1/T$. Where two or more molecules collide,
they must be activated before a reaction will occur. This is the basis
of the theory of activation energy from which Eq (9) is derived. This
theory requires that reactants must acquire enough energy to proceed
through an activation energy barrier in order to form products (Ref
28:623-24). Activation energy is thus another parameter which provides
quantitative values for comparing oxidation rates of various metals,
without concern over the individual mechanisms involved (Ref 21:6;
5:5).

When rate constants and activation energies are known for a par-
ticular range, the reactivity of the system at other temperatures
within that range can be interpolated.

Effects of Variables on Oxidation. The rate of deterioration of
a metal will be influenced by its service conditions, including such
variables as temperature, time, stress, and atmospheric conditions.

Generally, oxide growth increases with exposure time. Experi-
mental results which substantiate this statement are too numerous to
cite individually. The author noted that every experiment listed in
the bibliography revealed an increase in oxide thickness with time.
Emperical relations between time of exposure and oxidation rates were
presented on page 9 of this report.

In many cases, Arrhenius' equation may be used to represent the
effects of temperature on oxidation rates (Ref 49:25). Sartell's
and Li's (Ref 41:92) data on pure nickel is in close agreement with
this equation as well as Wlodek's data (Ref 51:5; 50:5) on Rene 41
and TD Nickel. In some complex reactions, however, the rate may de-
crease with an increase in temperature over certain ranges (Ref 43:
315), as seen by Wlodek (Ref 52: Fig. 4-5) in testing Udimet 700
between 1600 F to 1800 F, and in Hastelloy Alloy X between 1600 F to

13

1800 F beyond 1000 minutes. Cyclic or intermittent exposure to a constant temperature environment may result in more rapid oxidation due to oxide spalling cr cracking (Ref 24:115; 3:3). Miley (Ref 29: 264) states that in many instances intermittent heating and cooling results in higher oxidation rates due to spalling. The National Bureau of Standards (Ref 31:5) found that fluctuating temperatures caused greater depth of oxide penetration in a Ni-Mo-Cr alloy.

Oxide cluster formation caused by unequal local temperature distribution and surface conditions also will effect oxidation by changing available reaction areas, either increasing or decreasing rates (Ref 13:195).

There is little effect of stress on oxidation at very low creep rates. However, creep appears to be a factor which controls the rate of scaling, because at high stress levels, continual cracking of the oxide will occur, exposing more of the base metal surface to oxygen. The stress levels at which this cracking phenomenon becomes effective are difficult to define, for in certain metals such as nickel, creep rates are greatly reduced when oxide films form on their surface (Ref 33:31; 21:75). Miley (Ref 29:264, 292) states that stress-oxidation does not occur in nickel or Ni-Cr alloys exposed to air. Uhlig (Ref 48:234-35) theorizes that prior cold working has little effect on oxidation rates, but he says that oxidation rates do increase during strain. Richmond and Thorton (Ref 39:3), testing two Ni-Mo-Cr alloys, found that the depth of oxide penetration increased with increasing stress above a certain minimum, but that there was little effect of stress on oxidation rates at stresses below that required to produce one percent elongation in 100 hours. Examination of National Bureau of Standards' test data (Ref 31:5) indicates little effects of stress on oxidation rates for a 6‰ Cr, 13.5‰ Mo, 2‰ Ti, 1‰ Al, 1‰ Cb, 76‰ Ni alloy until very high loads at 1600 F to 1800 F. Their metallography does indicate an increase in depth of oxide penetration,

apparently from crack propagation. Siebert, et al (Ref 42:4-8) reported stress-oxidation of Chromel ASM and Hastelloy B after 100 hours during creep tests, however, when no creep occurred, little or no increase in oxidation was noted.

In processes where metal ions diffuse outward through oxide coatings, reductions in rates will be seen only at extremely low (below 1 mm Hg) oxygen pressures (Ref 17:396; 8:1149-50). Baur, et al (Ref 1:185) tested nickel from 1000 C to 1200 C at varying oxygen pressures and found oxidation rates insensitive to the changes. Wolk and Evans (Ref 53:129) found little change in internal oxidation in a Ni-1.04‰ Al alloy subjected to changing oxygen partial pressures, although a higher total weight gain was observed at higher partial pressures. Rhines (Ref 38:205) however, reported that when oxygen pressure is so low that external scale formed is quite thin, internal oxidation of copper alloys increased. For those systems which are pressure dependent, the rate constant can be expressed as

$$k = C P^V \tag{10}$$

where C is a proportionality constant, P is the partial pressure of oxygen and V is an experimentally determined constant which is less than one. This expression can be related to theories of chemical kinetics (Ref 32:7; 33:112).

Influences of geometry have been theorized by solution of the diffusion equation for spheres, cylinders, and flat plates (Ref 7: 441-50; 6:42-97; 40). These solutions show that a metal containing a limited amount of some easily oxidized alloying element, such as aluminum in Rene 41, will be markedly affected by changes in geometry. The initial rate of oxidation will increase with increases in wire diameter, but as depletion of available aluminum occurs, oxidation in smaller diameter wires will proceed more rapidly from diffusion of other alloying elements through the thinner Al_2O_3 layer formed. Initial oxidation

of the sheet will proceed by parabolic rates from initial exposure. Geometry, then, may greatly influence oxidation rates.

Mechanical Behavior of Oxides. The study of oxidation kinetics is further complicated in both pure metals and alloys by the mechanical behavior of reaction products. Normally, stresses will be formed at the metal-oxide interface, and between oxides, if the specific volume of each is different. This results from unequal thermal expansion of the oxides and substrate. The resultant stresses may then cause plastic deformation of the oxides just as in creep, culminating in cracks which expose more of the base metal to oxidation (Ref 37:2-3). The specific volume of the oxide also determines its adherency to the base metal through the relationship

$$Md/mD \qquad (11)$$

where m is the molecular weight of the metal, d is the density of the metal, M is the oxide molecular weight, and D is the oxide density (Ref 5:340). If

$$Md/mD > 1 \qquad (12)$$

then the oxide will be in compression on the surface of the metal with resultant adherence, as in the case of NiO and Al_2O_3 (Ref 10:134).

Pollock (Ref 35) stated that the oxide coat formed on TD Nickel is tenacious in nature and should not be expected to spall, and Manning, et al (Ref 27:11) noted no spalling of TD Nickel at rates up to and above 30 mg/cm^2. However, Gulbransen and Andrew (Ref 15:451) reported cracking and loss of scale while testing high purity nickel between 750 C and 1050 C. Wlodek (Ref 52:25) found exfoliation of Rene 41 scale whenever weight gain exceeded 1.5 to 2 mg/cm^2, and the same occurred to Udimet 700 above 0.8 mg/cm^2.

Nickel and TD Nickel. The oxidation of nickel in a constant test environment is a product of two major processes. The primary phase involves combination of oxygen and metal at the metal-gas interface by ordinary intermolecular forces, resulting in the formation of one or more oxide films (Ref 43:311). In the case of pure nickel, Arkharov (Ref 21:24), Sartell and Li (Ref 41:92), and Gulbransen and Andrew (Ref 15:451) have shown that only one type of oxide, NiO, is formed during oxidation in air. Additionally, they found two distinct layers of NiO with the same crystalline structure but with different lattice spacings. Wlodek (Ref 50:7-8) and Manning, et al (Ref 27:16-18) reported the same results for TD Nickel, except that at 1600 F Wlodek noted only the inner oxide coating. Both Wlodek and Manning found 2‰ ThO$_2$ in the inner oxide, but none in the outer layer. Smith (Ref 43: 313) disagrees and postulates that no two-phase layers will occur in an oxidation process except those which might form on cooling. Adsorption and the formation of an oxide results in a separation of the two reactants, nickel and oxygen, by the solid reaction product. The second phase, which proceeds almost simultaneously, involves the diffusion of oxygen inward and/or the diffusion of metal ions outward through the oxide where further reaction between the two occurs, thus building up the reaction product (Ref 33:93; 21:3; 43:312). Confusion clouds the mechanism that is rate controlling for nickel systems. Arkharov (Ref 21:24), for example, concluded from x-ray analysis of pure nickel at 1000 C that oxygen diffusing inwardly through the NiO lattice was predominant, but Sartell and Li (Ref 41:92), using inert marker techniques in the range 950 C to 1200 C, determined that diffusion of metal ions through the outer layer was rate determining. Manning, et al (Ref 27:18) postulated that the outer oxide layer in TD Nickel grows as a result of diffusion of metal ions outward, and that the inner oxide forms from diffusion of oxygen inward.

Nickel Alloys. Alloy systems oxidize ba ically by the same me-
chanisms as pure metals, that is, oxygen and metal combine at the
interface initially, then diffusion of oxygen and metal occurs through
the reaction zone. However, the nature of alloy oxidation will result
in new phenomena, such as selective oxidation and precipitation of
phases, which depend upon diffusion factors. These factors include
the activation energies for diffusion of each of the alloying elements,
concentration gradients of metal ions on both sides of the oxi :-metal
interface, and their coefficients of diffusion through the base metal
and oxides (Ref 21:73; 49:5; 5:241; 24:20-26).

Alloying elements requiring the lowest activation energies nor-
mally will oxidize first, depending on their degree of concentration
near the metal-oxide interface, and their velocity of movement through
the matrix (Ref 24:1-14). This was seen by Wlodek (Ref 51:16) during
oxidation of Rene 41 between 1600 F and 2000 F with the immediate
formation of Al_2O_3. Continuing oxidation then becomes a complex array
of reactions involving movement of less active metal ions to the
oxide coating, reactions between reactants, diffusion of reaction
products away from each other, and internal oxidation. Each of these
reactions create new bond energies between metal and oxygen or between
metal oxides which affects subsequent reaction rates (Ref 21:3).
Wlodek (Ref 51:16-23) noted the formation of a solid solution of (Al,
$Cr)_2O_3$ following the initial alumina (Al_2O_3) formation on Rene 41,
with continued chromium enrichment as the scale thickened. He con-
cluded that the growth of Cr_2O_3, containing Ni, Al, and other im-
purities, was the rate controlling process. Oxide cracking, and
diffusion of oxygen to the metal-oxide interface then permitted the
subscale formation of Al_2O_3 along grain boundaries. As oxidation
temperatures were increased, diffusion of nickel ions through Cr_2O_3
became appreciable, forming $NiCr_2O_4$, then NiO, over the Cr_2O_3. In
the same report, Wlodek found that Udimet 700 and Hastelloy Alloy X

oxides formed in a similar manner to Rene 41. Similarly, Pessl (Ref 34:18), in his examination of Fe-Cr-Y-Al oxidation data noted oxidation resistance from formation of Al_2O_3. Above 1000 C. however, he found that aluminum loss was high with resultant preferential oxidation of chromium. Ignatov and Shamgunova (Ref 21:74) examined an 80% Ni-20% Cr alloy and found that the oxide film formed in three stages commencing with a thin layer of NiO, followed by diffusion of Cr and Ni to form $NiCr_2O_4$. Then due to oxygen starvation close to the metal-oxide interface, $NiCr_2O_4$ was reduced by chromium, resulting in a double layer of $NiCr_2O_4$ and Cr_2O_3. Extensive internal oxidation occurred from selective oxidation of chromium by the oxygen in the spinel ($NiCr_2O_4$ crystalline structure).

Rate Measurement Techniques

The most common method used to evaluate oxidation rates is the gravimetric method, by which rates are determined through weight change measurements over periods of time under constant environmental conditions (Ref 24:88; 10:752; 21:8-9). The periodic weight increase equals the mass of oxygen consumed. Weight change measurements may be made continuously by suspending the specimens from an inert suspension system which is attached to an analytical balance; this type and more sophisticated "thermobalances" are discussed extensively in the literature (Ref 24:88-92; 21:8-9).

Major problems encountered with a "thermobalance" are thermal currents from the furnace hot zone, buoyancy effects from furnace drafts (Ref 49:3), and air currents from movement in the vicinity of the test area (Ref 21:9). This author originally designed his test apparatus for employment of a "thermobalance", but discarded the plan after encountering all of the problems cited above. Another form of gravimetric measurement is direct, intermittent weighing on an analytical balance after repeated exposures to the test environment (Ref

24:89). The disadvantage of this method is that upon cooling, cracking and spalling of some oxides may occur (Ref 21:9).

A third weighing technique involves removal of the oxide scale, after exposure, by pickling. The loss in weight is then measured. The danger in this method is that pickling may damage the metal surface (Ref 5:344), resulting in erroneous weight loss measurements.

Metallographic techniques may be employed to evaluate rates of oxidation by measurement of the depths of internal oxide penetration, measurement of oxide thicknesses, and depths of alloy depletion in the base metal (Ref 24:84-86).

Other techniques for studying oxidation rates are covered extensively in an excellent review by Kubaschewski and Hopkins (Ref 36:80-118).

III. Experimental Apparatus and Procedures

Test Equipment

Specimens were exposed to test environments in 1 1/2" diameter by 24" long alumina tubes which were inserted into two vertical creep furnaces and a horizontal globar furnace. Specimens were suspended in the test apparatus from a Rene 41 rod, one end of which was machined into a vice grip. Specimens to be placed under stress were clamped to a second rod which extended through an aperature in the base of the alumina tube. Calibrated weights were then attached to this rod. During controlled atmospheric testing, the alumina tubes were sealed with a stainless steel plug fitted with a gas outlet port. A gas inlet port was machined in the base of the alumina tube. The general layout of a typical test fixture is shown in Fig. 2.

Temperature control in a 3" hot zone was maintained to within $\pm$ 5 F by using Wheelco controllers. Voltage regulators on the input power lines eliminated voltage fluctuations. All furnace and specimen thermocouples used in this experiment were alumel-chromel, calibrated against an NBS certified platinum-platinum, 10% rhodium thermocouple. Temperature readings were made periodically with a Leeds and Northrop multiple-range potentiometer, and continuous temperature readings were recorded on a Bristol-Dynamaster four-channel recorder every 30 seconds.

Commercial oxygen and argon were used for controlled atmospheric testing, with flow control maintained by Brooks "Rotameter" flowmeters. The argon was purified (Fig. 3) by passing the gas through magnesium perchlorate and silica gel drying towers. The gas was then passed through a 1" diameter stainless steel tube, filled with a titanium chip getter which was heated to 1600 F by a globar furnace. Finally the gas was directed through another silica gel drying tower and a liquid-nitrogen trap prior to passage through the flowmeter and into the test chamber (Ref 26:2095-6).
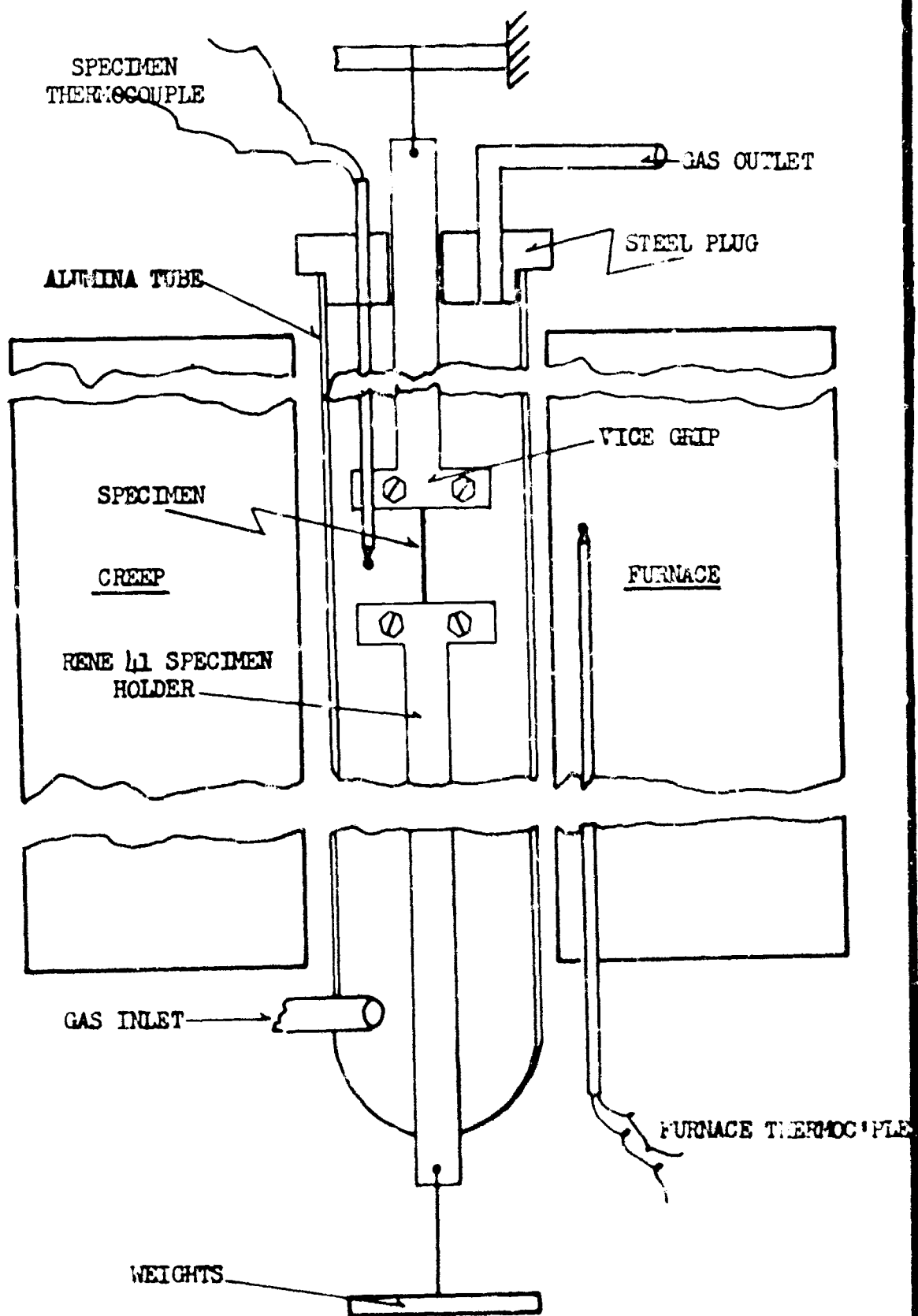
FIG. 2 ARRANGEMENT OF TYPICAL TEST APPARATUS (not to scale)

22
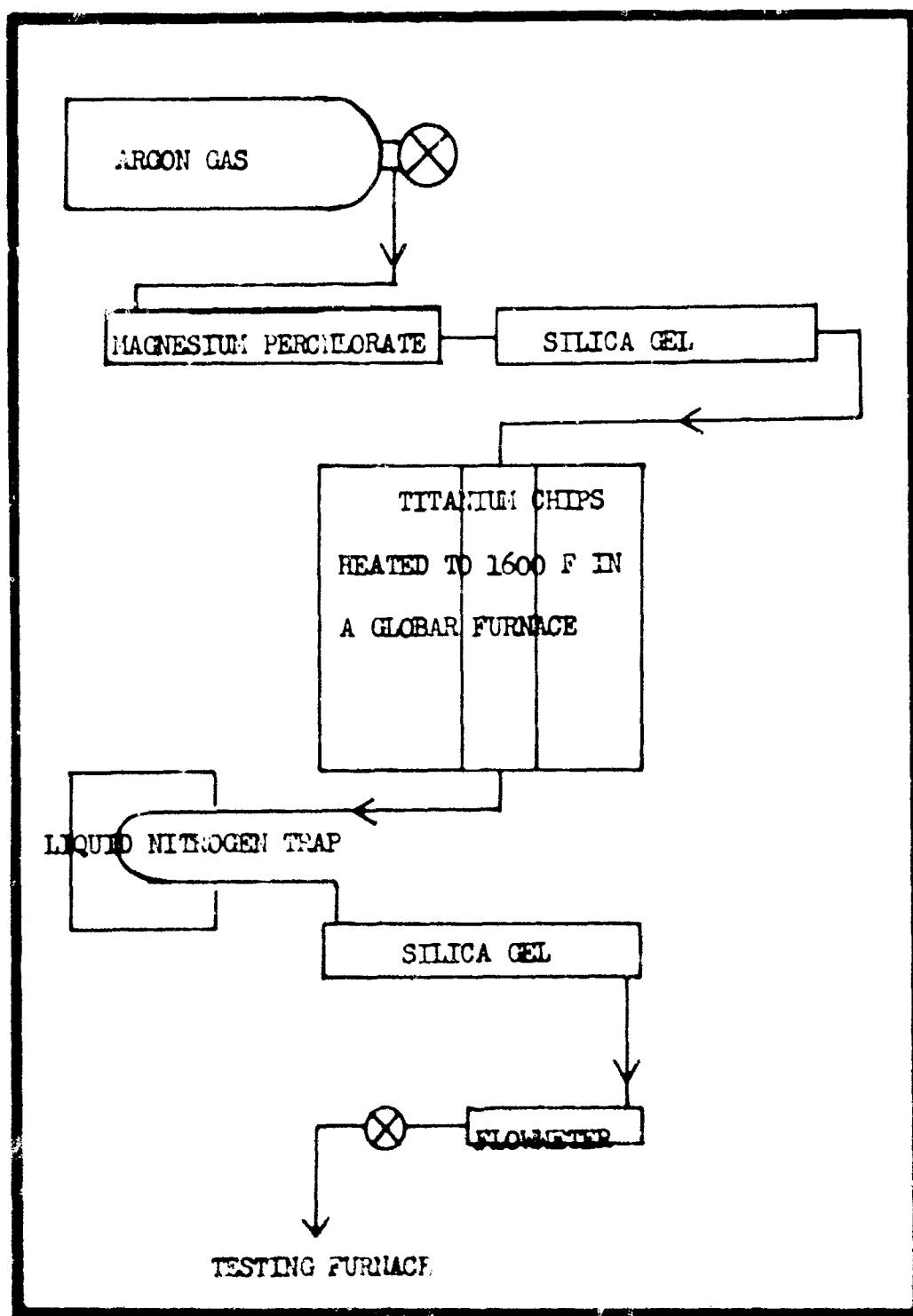
FIG. 3   ARGON PURIFYING TRAIN

23

Weight-change measurements were made by direct weighing of the specimen on a Voland Analytical Balance accurate to 0.025 milligrams. The analytical balance scale was magnified to facilitate readings and to achieve more accuracy.

Procedures

Gravimetric methods (Ref 35:88-92) were used to obtain weight-gain data during oxidation experiments with 0.50" x .05" Rene 41 sheet, .01" and .02" diameter Rene 41 wire, and .01" and .02" diameter TD Nickel wire. Specimen compositions are given in Table I.

TABLE I

Composition of Test Materials, ‰

Rene 41	C	Mn	Si	Cr	Ni	Mo	B	Co	Fe	S	Ti	Al
.01" Wire	.09	.10	.05	18.90	Bal	9.6	.003	11.64	.50	.008	3.14	1.55
.02" Wire	.09	.10	.05	18.90	Bal	9.6	.003	11.64	.50	.008	3.14	1.55
.05" Sheet	.09	.10	.05	19.00	Bal	9.9	.004	11.50	.50	.008	3.10	1.50

TD Nickel	Ni	ThO_2	Impurities
	98	2.0	Undetectable by spectroscopic analysis

Rene 41 specimens were prepared for testing by abrading the surface with 600 grit emory paper, then washing the specimens in ethanol. Initially, TD Nickel wires were prepared in the same manner, but erroneous oxidation data was obtained in view of the fact that foreign material had been cold worked into the surface during the wire drawing process. To eliminate this impurity problem, the wires were abraded as previously described, then electropolished in an electrolyte of 1 part H_2SO_4 and 7 parts ethyl alcohol.

Wires .01" and .02" diameter were cut to 12" and 6" lengths, respectively, for no load testing. Because of test zone limitations, specimens to be stressed were by necessity limited to 3" in length.

Ragged edges were ground off to reduce possible edge effects, then the specimens were measured to determine diameters and lengths, necessary for the calculation of total surface areas. Prior to obtaining the initial weight measurements, the specimens were given a final cleaning in acetone to remove any contamination from handling.

Coiled no-load specimens, and sheet specimens were then lowered into the test furnaces. Uncoiled specimens for stress testing were attached to the suspension system and after the specimen was lowered into the hot zone of the furnace the weights were applied. At random time intervals, the specimens were removed from the furnace, air cooled, and reweighed. This process was repeated for varying time periods up to 1000 minutes, or until spalling of the specimen was detected.

Prior to controlled-atmospheric testing, a positive overpressure of argon at a rate of 10 cfh was established in the test chamber. After lowering the specimen into the hot zone, argon and oxygen flows were regulated to the desired ratio, and a combined flow rate of 3 cfh was maintained.

Oxidation testing was followed by metallographic examination of specimens, which were mounted, polished, and etched in a flowing solution of 150 ml H_2O, 30 ml H_2SO_4, 360 ml HCl, 100 ml HNO_3, 150 ml HAc and 90 gm $FeCl_3$ (Ref 52:7). After etching, which exposed the depth of alloy depletion, measurements of Rene 41 depletion depth were correlated with observed rate data. In addition, NiO, which was formed on the surface of TD Nickel during exposure, was measured for thickness to substantiate rate data.

Upon completion of these oxidation tests and measurements, a solution for the apparent oxidation rates was performed on the IBM 7090-7094 computer.

During the latter stages of testing, a"thermobalance" with automatic weight-change recording capabilities was used for isothermal

oxidation measurement of wire specimens. These tests were performed to determine the effects, if any, of thermal cycling encountered in the earlier tests, and to accurately measure very early weight changes.

IV. Presentation and Discussion of Results

Oxidation data is presented in this section in the form of log-log and linear curves, plotting time in minutes versus weight gain per unit area in milligrams per square centimeter. Actual weight gain measurements for each test may be found in Appendix A. The values computed for the rate constant, K, and the inverse slope of the log-log curves, which represents the power exponent, b, in Eq (1) are tabulated in Appendix B along with the total variance of Δm for each set of data.

Rene 41 Oxidation

Sheet. Initial oxidation data obtained by this author for Rene 41 wire deviated significantly from the theoretical parabolic rate constant which has been demonstrated experimentally for Ni-Cr alloy sheet by many previous investigators. Consequently, a series of oxidation tests on Rene 41 sheet was performed in an effort to validate the test procedures employed. The results of these tests, shown in Fig. 4 compared favorably with the expected parabolic oxidation law,

$$\Delta m^2 = K t + C \tag{4}$$

Actual values for the power exponent for Δm determined by the IBM 7090-7094 computer were 2.3 at 1600 F, 2.0 at 1700 F, and 2.3 at 1800 F. This data compares favorably with the results obtained by Wlodek (Ref 51: Fig. 1) also presented in Fig. 4. Metallographic examination of Rene 41 sheet (Fig. 5) revealed the same increasing depth of alloy depletion with temperature noted by Wlodek (Ref 52:64). Differences in rates, particularly at 1600 F, can be attributed to different test conditions, such as the location of specimen thermocouples to measure temperature and different heat treatments. Additionally, Wlodek's specimens were not subjected
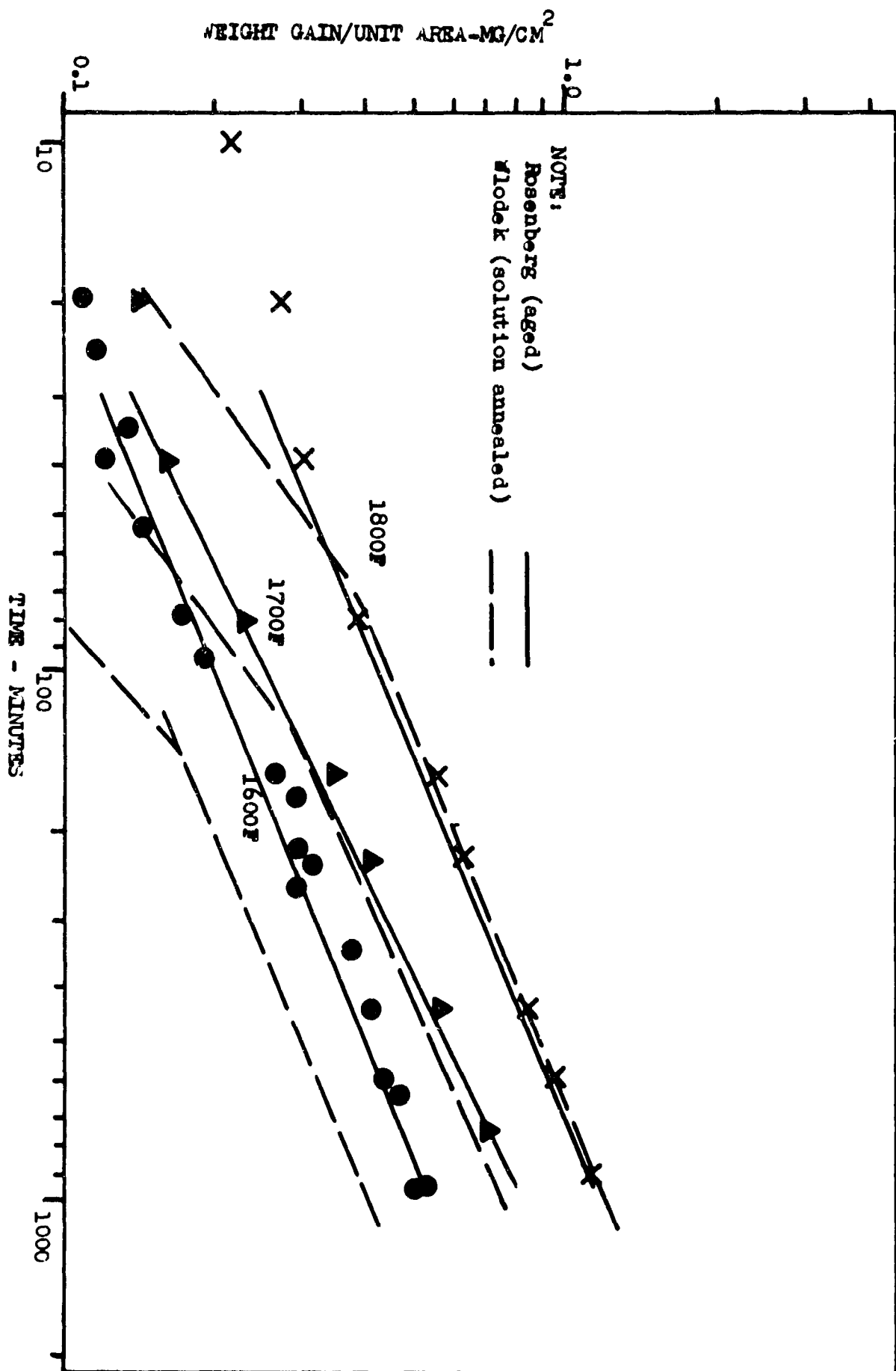
FIG.4   OXIDATION DATA FOR RENE 41 SHEET (50 mil thick)
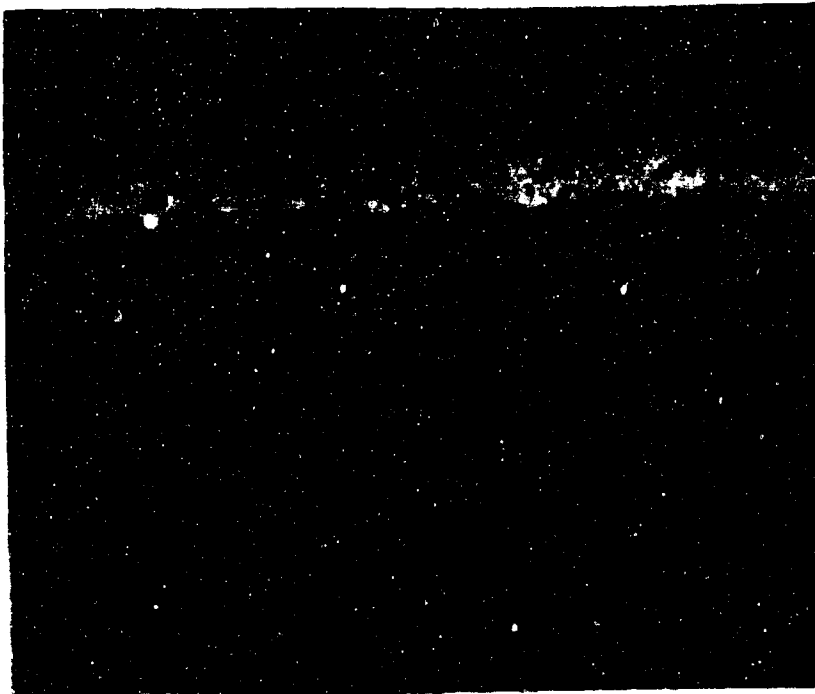
Rene 41 50 mil sheet   1600 F
Mag. 500 X
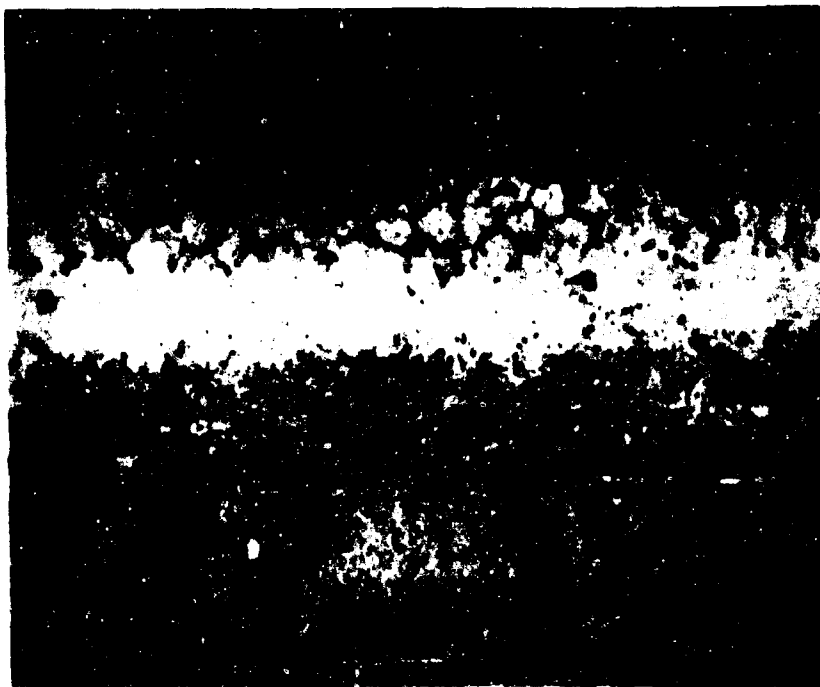
Rene 41 50 mil sheet   1800 F
Mag. 500 X

Fig. 5
Oxidation of Rene 41
50 mil sheet at 960 minutes

to thermal cycling, which could account for his lower initial data points, and the displaced slope for 1600 F. Within the limits of accuracy attainable in an experiment of this type, the author concluded that parabolic oxidation had taken place, validating the original procedure used to oxidize and evaluate wires.

Wire. Curves showing the oxidation of 10 mil (0.01") and 20 mil (0.02") Rene 41 wire are shown in Figs. 6 and 7. These curves show that oxidation in both wire diameters proceeds at a much slower rate than if the oxidation phenomenon obeyed a parabolic law. Attempts were made by the author to establish an empirical relationship between weight gain and time by plotting test data on various type of graph paper, a common method employed to develop empirical equations (Ref 25:Ch6). The best approximation to a straight-line presentation of data was obtained by the type of plot used in Figs. 6 and 7, which is a log-log display.

Comparison of Wire and Sheet. As noted previously, the oxidation of the wires proceded at markedly different rates from the oxidation of sheet material. In order to make a reasonable comparison between sheet and wire, and between different wire diameters, the IBM 7090-7094 computer at ASD was used to determine the slope of each oxidation curve and its associated rate constant. A least squares program was used to solve the equation

$$\Delta m^b = kt \tag{1}$$

in that the oxidation observed was best described by the power series law. A computer program was used to minimize the value of

$$\Sigma \left[b \log \Delta m - \log kt \right]^2 \tag{13}$$
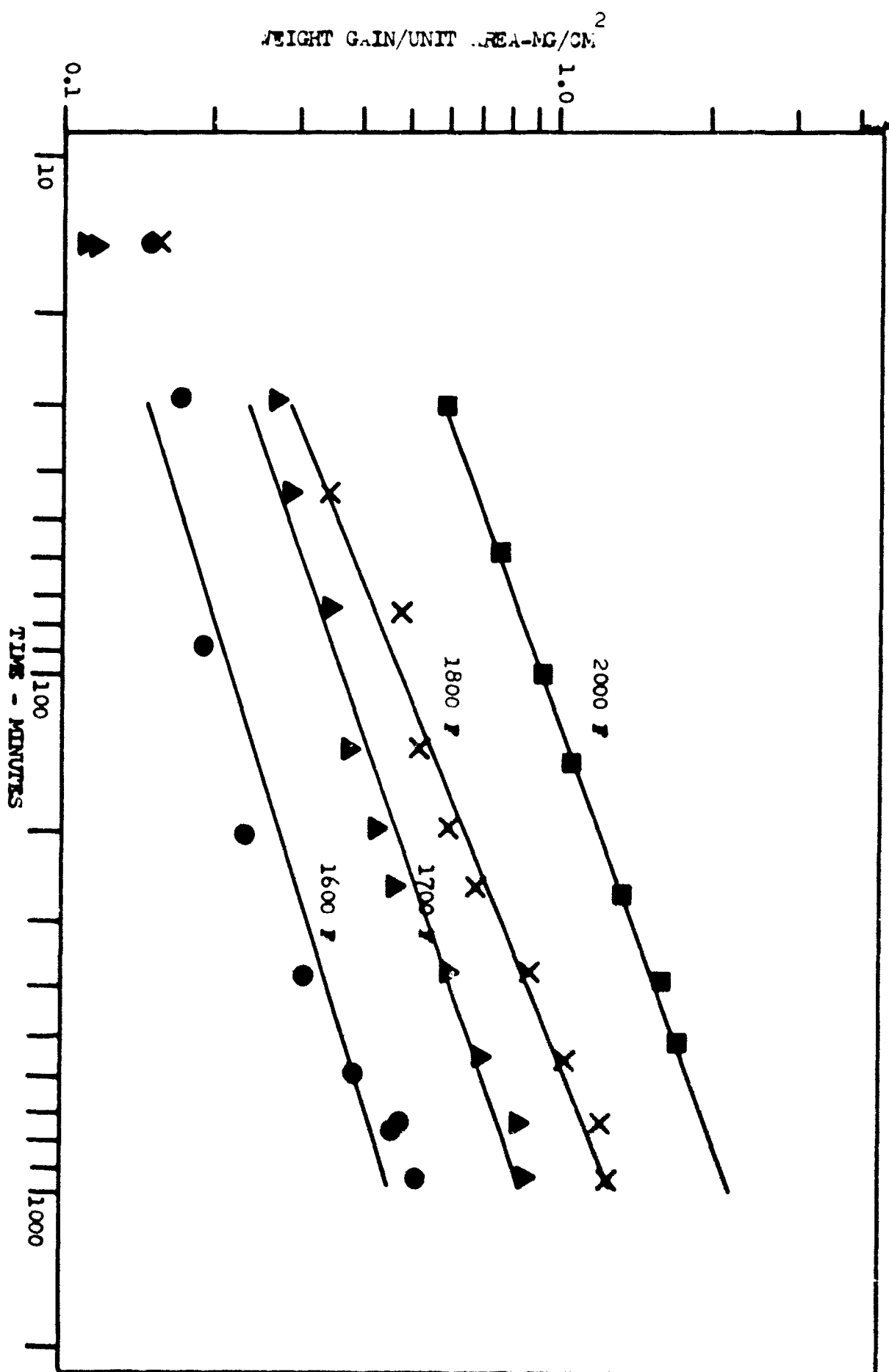
FIG. 6   OXIDATION DATA FOR RENE 41   (10 ml air)

FIG. 7   OXIDATION DATA FOR RENÉ 41   (20 mil wire)

and to determine the variance of the

$$\sum \left[(kt)^{1/b} - \Delta m \right]^2 \tag{14}$$

in order to establish some confidence level in the data scatter for values of Δm.

The power exponent computed for 10 mil wire ranged from 3 at 1600 F to 2.4 at 1800 F, and from 8.6 at 1600 F to 3.8 at 2000 F for 20 mil wire. These exponents and their corresponding rate constants revealed much higher initial weight gain in 20 mil wire, followed in magnitude by 10 mil wire, and then by sheet. As exposure time continued, however, rates of oxidation proceeded in inverse order with sheet material oxidizing most rapidly. Figs. 8 and 9 graphically illustrate the difference in oxidation rates at 1600 F and 1700 F. Similar phenomenon was noted at 1800 F and for wires only at 2000 F. (No sheet was oxidized at 2000 F.)

Analysis of Rates. Since diffusion of metal ions first to the metal-gas interface, and later through the metal and oxide to the oxide-gas interface are considered to be rate controlling processes for Ni-Cr alloys of this type (Ref 24:198; 52:19), Fick's laws for diffusion are appropriate for analysis of this data. Darkin and Gurry (Ref 7:441-450), and Crank (Ref 6:42-97) have solved the diffusion equation for various geometric shapes, including cylinders and sheets, which satisfy the results obtained in this experiment. An interesting approach to the same problem was performed by Sansom (Ref 40) who solved the differential equation

$$\partial C / \partial t = D \nabla^2 C \tag{15}$$
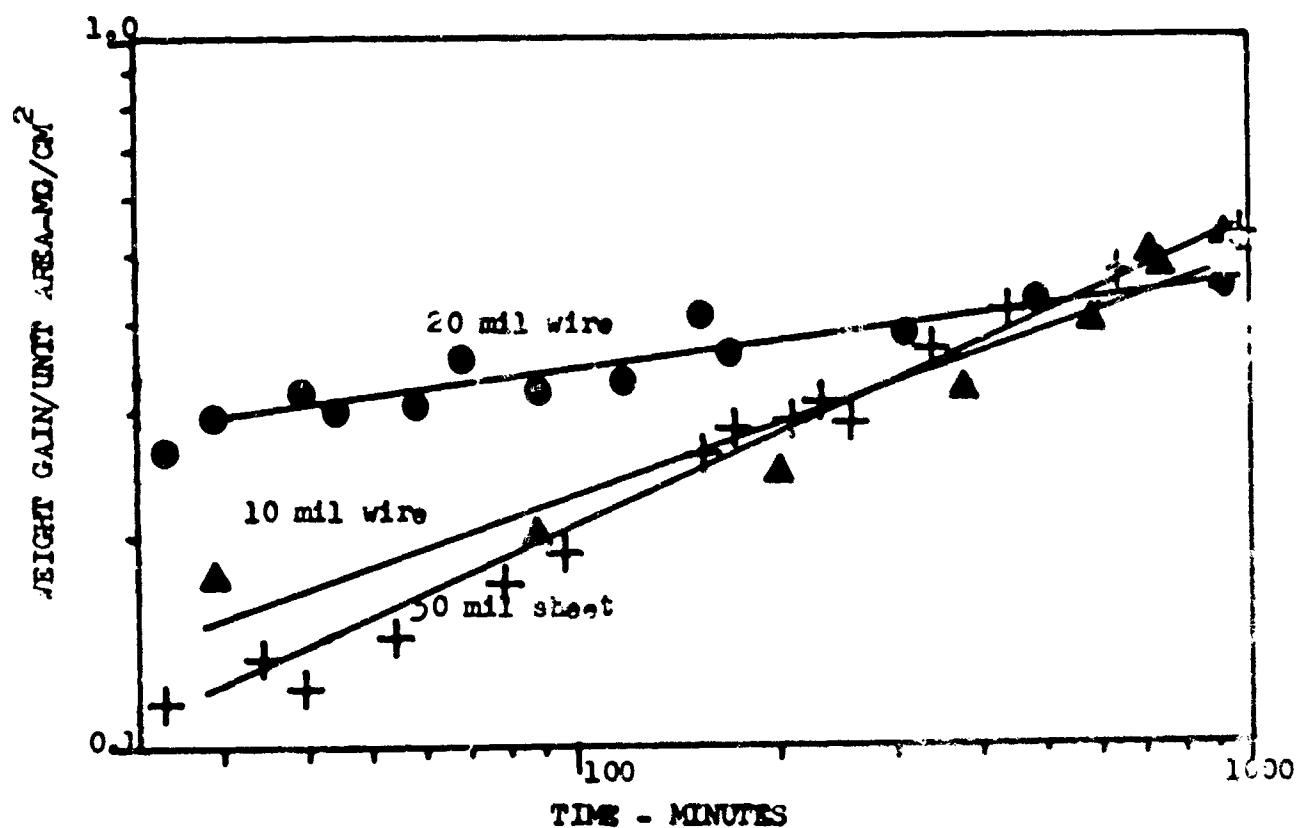
FIG. 8   EFFECT OF GEOMETRY ON OXIDATION OF RENE 41 AT 1600 F
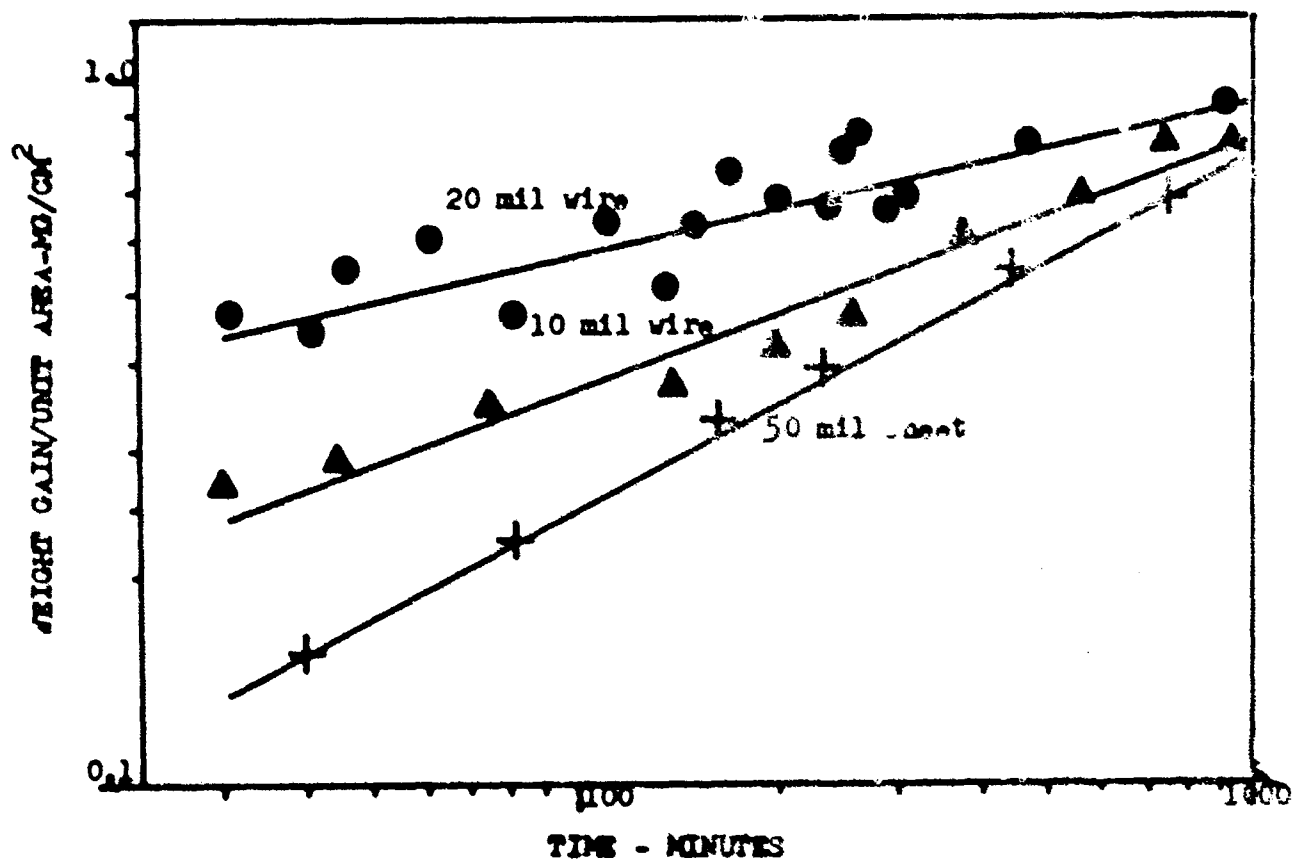
FIG. 9   EFFECT OF GEOMETRY ON OXIDATION OF RENE 41 AT 1700 F

where C was equal to temperature, for diffusion of a finite amount of
heat through a 16 mil wire being quenched from a high temperature.
This expression is Fick's second law, Eq (8), written in vector nota-
tion, assuming that D is independent of concentration (R f 7:445).

Sansom's solution is well suited to this author's problem, in
that the amount of aluminum in the Rene 41 wire available for diffusion
and subsequent oxidation is finite and uniformly distributed, just as
the initial heat content in Sansom's problem was finite and uniformly
distributed. In Rene 41, it will be assumed that less than 15‰ of the
total aluminum (1.5%) in the alloy is available for diffusion in the
early stages of oxidation (less than 10 minutes). The remainder of
the aluminum is retained in the intermetallic compound, $Ni_3(Al,Ti)$ and
is not available for oxidation. These assumptions have been experiment-
ally verified by metallographic measurement of the depth of aluminum
depletion by this author and Wlodek (Ref 51: Fig. 11). X-ray analysis
and tensile-test data substantiate the presence of $Ni_3(Al,Ti)$.

The approximation will be made in this analysis that the oxidation
of aluminum proceeds independently of the formation of chromia, and
that a thin film of Al_2O_3 is formed before the commencement of chromium
oxidation. These assumptions are justified by the much higher free
energy of formation of Al_2O_3 over Cr_2O_3 (Ref 7:349). This causes the
oxide-gas interface to be reducing to chromium ions as long as aluminum
is available at the surface.

By assuming that aluminum diffusion in Rene 41 is mathematically
similar to heat diffusion in wire, in that both processes obey Fick's
law, the slopes of Sansom's analog computer plots (Ref 40: Fig. 5) of
concentration (temperature) versus time may be integrated to give the
accumulation of aluminum at the surface of the wire. This accumulation
of aluminum may be represented graphically as aluminum concentration
at the surface versus time for a particular wire diameter. For any

smaller wire diameter

$$C = f(Dt/X^2) \qquad \text{(Ref 7:445)} \quad (16)$$

where C is the accumulation of aluminum at the surface, D the diffusion constant, t the time, and X the characteristic dimension of the specimen; thus the aluminum in the smaller wire will diffuse approximately

$$X_2^2 / X_1^2 \qquad (17)$$

times more rapidly than in the larger wire. X_2 represents the radius of the larger wire and X_1, the radius of the smaller wire. This means that if accumulation versus time is plotted for aluminum diffusion in 10 and 20 mil wires, the result would appear as in Fig. 10, plotted in non-dimensional co-ordinates for simplicity.

Simultaneously, it must be considered that for two equal surface areas of 10 and 20 mil wire, the total volume of the 10 mil wire is one-half that of the 20 mil wire, therefore the total amount of aluminum available for oxidation in the 10 mil wire is also one-half as much. If Fig. 10 is converted to a graphical representation of Al_2O_3 thickness versus time, caused by oxidation of aluminum, the accumulation of aluminum for 10 mil wire at any time, t must be divided by 2 for comparison with 20 mil wire of the same surface area, as shown in Fig. 11.

The symbols and definitions to be used for the remainder of this analysis are:

J^{Cr} = Flux of chromium ions $(mg/cm^2\text{-min})$

D^{Al} = Diffusion constant for chromium ions through Al_2O_3 (cm^2/min)

D^{Cr} = Diffusion constant for chromium ions through Cr_2O_3 (cm^2/min)
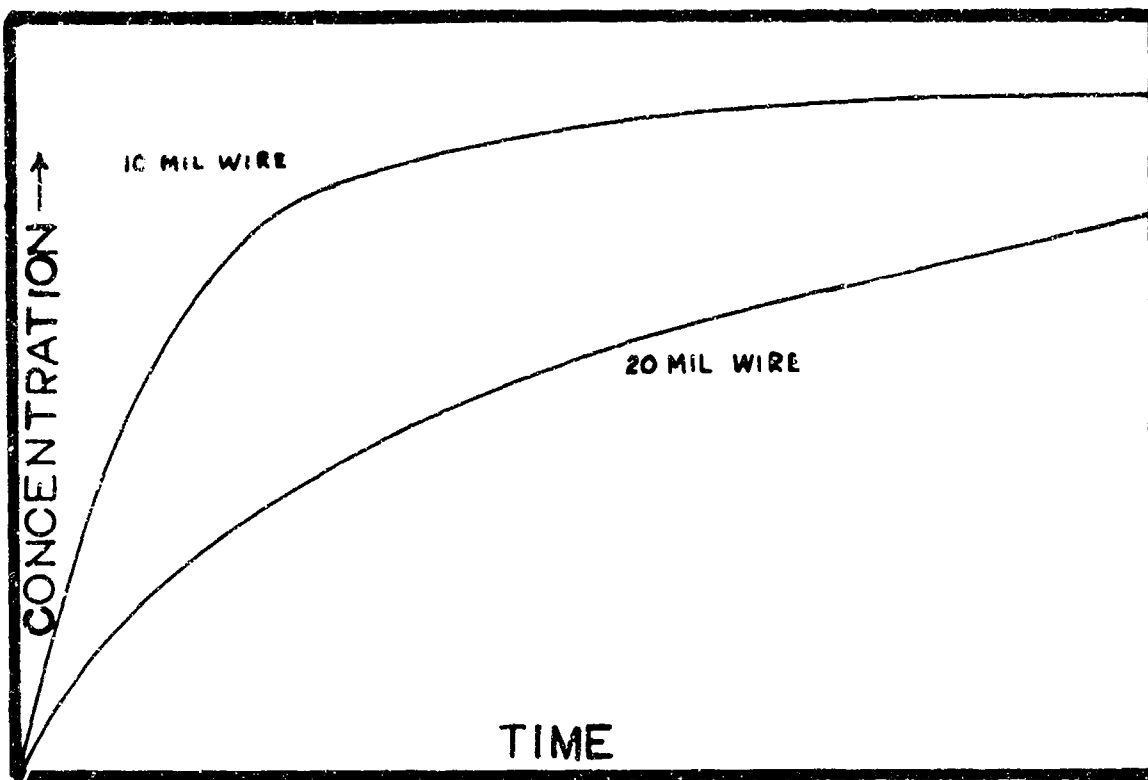
Fig. 10   Al Concentration at Rene 41 wire surface vs. time
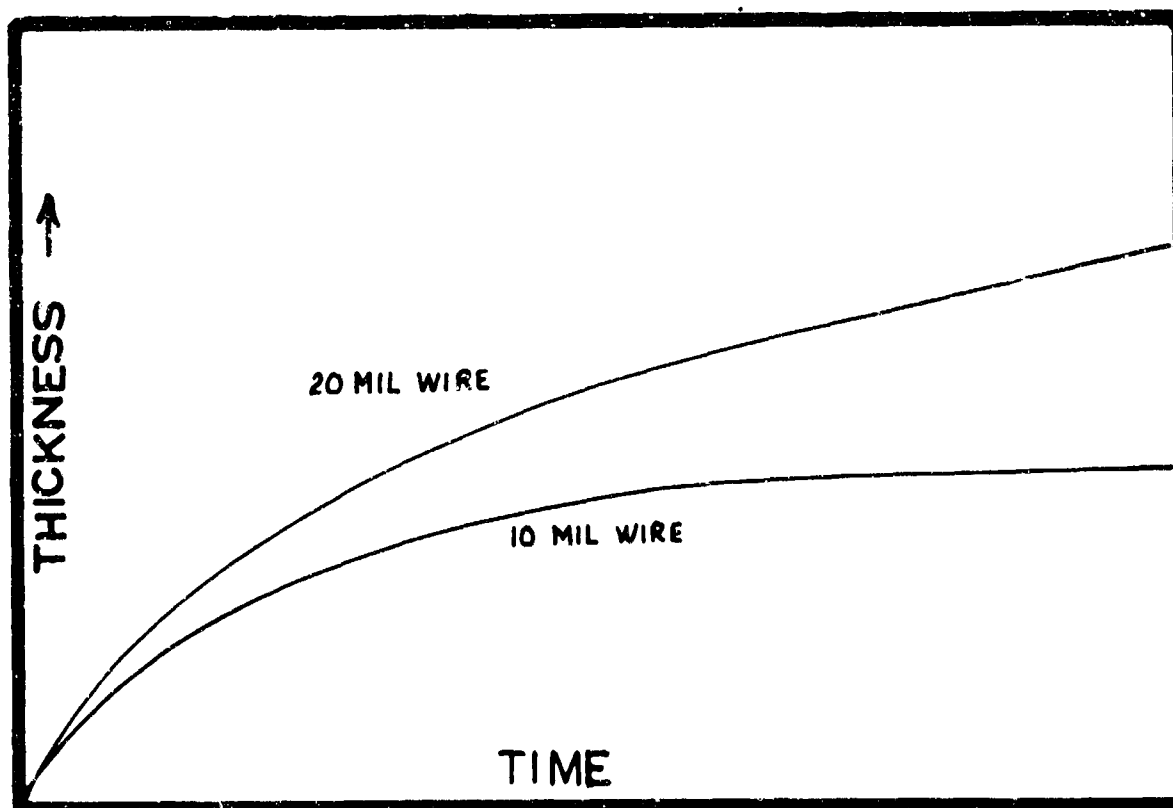
Fig. 11 Al_2O_3 Thickness on Rene 41 wire vs. time

37

ΔC^{Al} = Change in concentration of chromium ions across Al_2O_3

(mg/cm^3)

ΔC^{Cr} = Change in concentration of chromium ions across Cr_2O_3

(mg/cm^3)

(mg/cm^3)

ΔX^{Al} = Change of Al_2O_3 thickness during an incremental time (cm)

ΔX^{Cr} = Change of Cr_2O_3 thickness during an incremental time (cm)

ρ^{Cr} = Density of Cr_2O_3 (mg/cm^3)

X^{Cr} = Thickness of Cr_2O_3 (cm)

X^{Al} = Thickness of Al_2O_3 (cm)

$1,2,\ldots i$ = Subscript denoting a time interval

t = Time (minutes)

Δt = Increment of time

m = Mass (mg)

Δm = Increment of mass (superscript Cr denotes chromium)

A = Area (cm^2)

Now it is necessary to determine the effect of the Al_2O_3 oxidation

rates on the formation of Cr_2O_3, since chromium will be oxidizing at the

same time, but more slowly, than aluminum. Diffusion of chromium

through Al_2O_3 will be rate controlling for this process, in that

$$D^{Cr} \gg D^{Al} \qquad \text{(Ref 21:54)} \qquad (18)$$

An expression for the change in Cr_2O_3 thickness as a function of time

may be derived from Fick's laws, employing a finite difference mathe-

matical approximation.

The flux of chromium, J^{Cr}, through a unit area of oxide can be

approximated initially as

$$J_i^{Cr} = D^{Al} \Delta C_i^{Al} / \Delta X_i^{Al} \qquad (19)$$

where ΔC_1^{Al} can be represented graphically (Fig. 12) by a gradient line from the metal surface to air across Al_2O_3. Also

$$J = d(m/A)/dt \qquad (20)$$

or

$$J\Delta t = \Delta m/A \qquad (21)$$

for incremental times, assuming

$$A \neq f(t) \qquad (22)$$
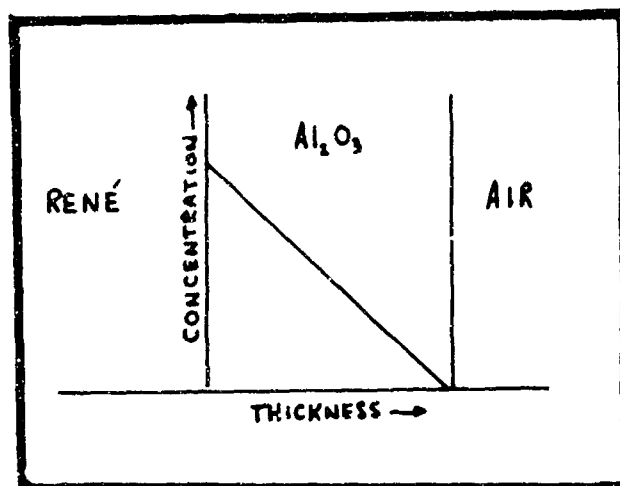
Further

Fig. 12

Gradient of Chromium across Al_2O_3

$$\Delta m^{Cr}/A = \varrho^{Cr}\Delta X^{Cr} \qquad (23)$$

Substituting Eqs (19) and (21) in Eq (23)

$$\Delta X_1^{Cr} = \left(D^{Al}\Delta C_1^{Al}\Delta t_1\right)/\left(X_1^{Al}\varrho^{Cr}\right) = X_1^{Cr} \qquad (24)$$

For the second time increment, Δt_2, the flux across Cr_2O_3 will equal the flux across the Cr_2O_3 formed during Δt_1, or

$$\left(D^{Al}\Delta C_2^{Al}\right)/X_2^{Al} = \left(D^{Cr}\Delta C_1^{Cr}\right)/X_1^{Cr} = J \qquad (25)$$

The total change in concentration ΔC, which is constant because of an infinite chromium source, will be represented graphically (Fig. 13) by a gradient line across Al_2O_3 and Cr_2O_3, where

$$\Delta C = \Delta C_2^{Al} + \Delta C_1^{Cr} \qquad (26)$$
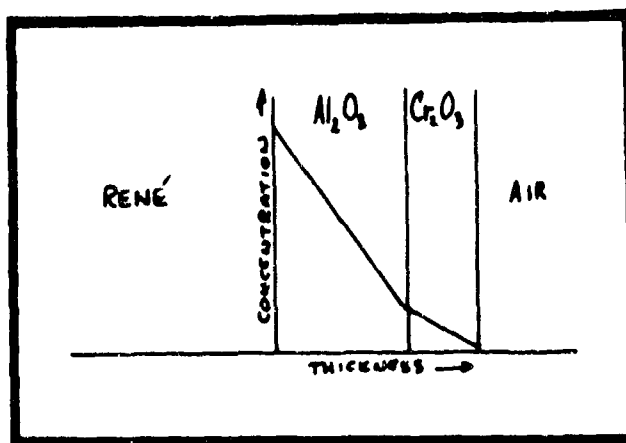
Fig. 13

Gradient of Cr across Al_2O_3 + Cr_2O_3

Substituting Eq (26) in Eq (25)

$$(D^{Al}\Delta C_2^{Al})/\chi_2^{Al} = \left[(D^{Cr}\Delta C)/\chi_1^{Cr}\right] - \left[(D^{Cr}\Delta C_2^{Al})/\chi_1^{Cr}\right] \quad (27)$$

whence
$$\Delta C_2^{Al} = (D^{Cr}\Delta C \, \chi_2^{Al})/(D^{Cr}\chi_2^{Al} + D^{Al}\chi_1^{Cr}) \quad (28)$$

Substituting Eq (21), (25), and (28) into Eq (23)

$$\Delta \chi_2^{Cr} = (D^{Al}D^{Cr}\Delta C \Delta t_2)/[(\rho^{Cr})(D^{Cr}\chi_2^{Al} + D^{Al}\chi_1^{Cr})] \quad (29)$$

from which
$$\chi_2^{Cr} = \chi_1^{Cr} + \Delta \chi_2^{Cr} \quad (30)$$

or in general
$$\Delta \chi_i^{Cr} = (D^{Al}D^{Cr}\Delta C \Delta t_i)/[(\rho^{Cr})(D^{Cr}\chi_i^{Al} + D^{Al}\chi_{i-1}^{Cr})] \quad (31)$$

and
$$\chi_i^{Cr} = \sum^{i}_{i} \Delta \chi_i^{Cr} \quad (32)$$

Substituting values of χ_i^{Al} from Fig. 11 and values of D from the
literature, it can be shown that the diffusion of chromium through
Al_2O_3, with the resultant formation of Cr_2O_3, will proceed more rapidly
in the smaller diameter wire as shown in Fig. 14. This is intuitively
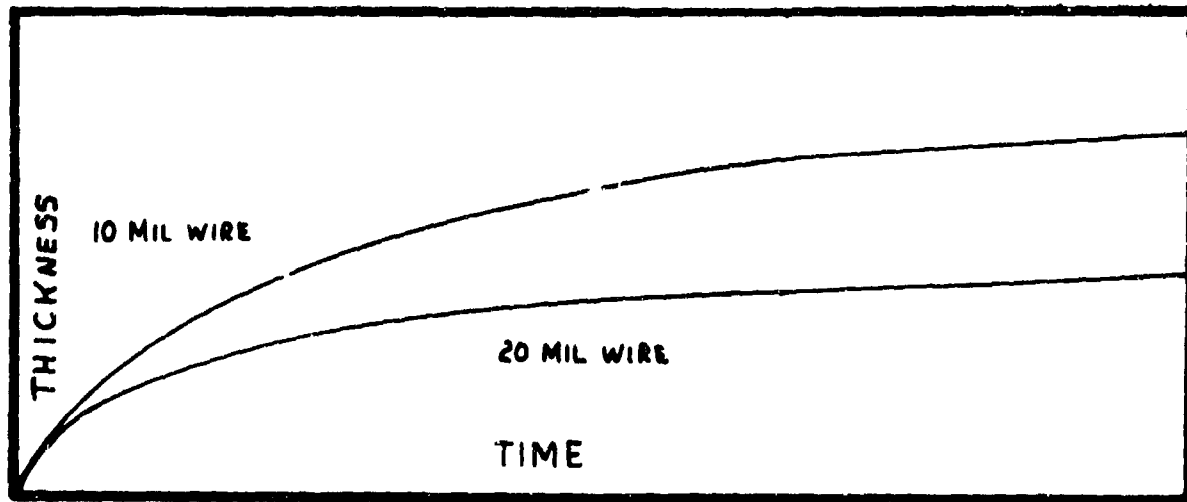
Fig. 14   Growth of Cr_2O_3 over Al_2O_3 in Rene 41 wires

obvious since the Al_2O_3 on the 10 mil wire is not as thick as Al_2O_3 on
the 20 mil wire.

In that
$$\Delta m /A = \rho \Delta X \tag{21}$$

the graphs of thickness versus time (Figs. 11 and 14) may be converted to weight gain of O_2/unit area versus time. A summation of the resultant curves should approximate the true weight gain for the system.

Examining the early oxidation process,

$$\Delta C_i^{Al} \gg \Delta C_{i-1}^{Cr} \tag{33}$$

therefore, from Eq (25)

$$D^{Cr} X_i^{Al} \gg D^{Al} X_{i-1}^{Cr} \tag{34}$$

making
$$\Delta X_i^{Cr} = (D^{Al}\Delta C \Delta t_i)/(X_i^{Al}\rho^{Cr}) \tag{35}$$

in Eq (31), which approaches a linear rate as X_i^{Al} proceeds to its limit.

For the intermediate case, when

$$\Delta C_i^{Al} \approx \Delta C_{i-1}^{Cr} \tag{36}$$

hence
$$D^{Cr} X_i^{Al} \approx D^{Al} X_{i-1}^{Cr} \tag{37}$$

therefore
$$\Delta X_i^{Cr} = (D^{Al}\Delta C \Delta t_i)/(2 X_i^{Al}\rho^{Cr}) \tag{38}$$

in Eq (31), showing that ΔX_i^{Cr} decreases with time.

During late oxidation, when

$$\Delta C_i^{Al} \ll \Delta C_{i-1}^{Cr} \tag{39}$$

$$D^{Cr} X_i^{Al} \ll D^{Al} X_{i-1}^{Cr} \tag{40}$$

making
$$\Delta X_i^{Cr} = (D^{Cr}\Delta C \Delta t_i)/(X_{i-1}^{Cr}\rho^{Cr}) \tag{41}$$

in Eq (31). This last expression represents a parabolic process.

Thus, the oxidation of Rene 41 wire can be summarized as a three step process consisting of:

1. Asymptotic growth of Al_2O_3;

2. Asymptotic growth of Al_2O_3 and linear growth of Cr_2O_3;

3. Parabolic growth of Cr_2O_3.

Comparing actual data from thermobalance oxidation tests (Fig. 15) with the above theory; it can be seen that a knee does occur in the 10 mil curve approximately four times faster than for the 20 mil curve, in agreement with the ratio

$$ X_2^2 / X_1^2 \qquad (17) $$

This corresponds to the rapid diffusion caused by the higher concentration gradient of aluminum in the 10 mil wire. The fact that there is more aluminum in the 20 mil wire accounts for the higher weight gain noted on the initial portion of Figs. 8, 9, and 15. As diffusion and oxidation of chromium become rate controlling earlier in the 10 mil wire, the 10 mil wire slopes should be higher than the 20 mil slopes, accounting for the difference between the two actual curves. Johnson, et al (Ref 22:6-14) found similar results for short time test results during 10 minute oxidation studies of 0.5 to 5 mil Ni-Cr-Al superalloy wires.

The wire curves resulting from actual experiment do exhibit the same general properties, then, as the theoretical curves. The theory, however, cannot be extended for the entire duration of the process, in that the actual oxidation mechanism becomes more complex as time proceeds. A third variable, the diffusion of nickel, resulting in the formation of $NiCr_2O_4$ and possibly NiO, must be considered. Again considering only the early stages of oxidation, the difference in concentration gradient across the two wire diameters plays a significant role in the process. The sheet material, however, because of its
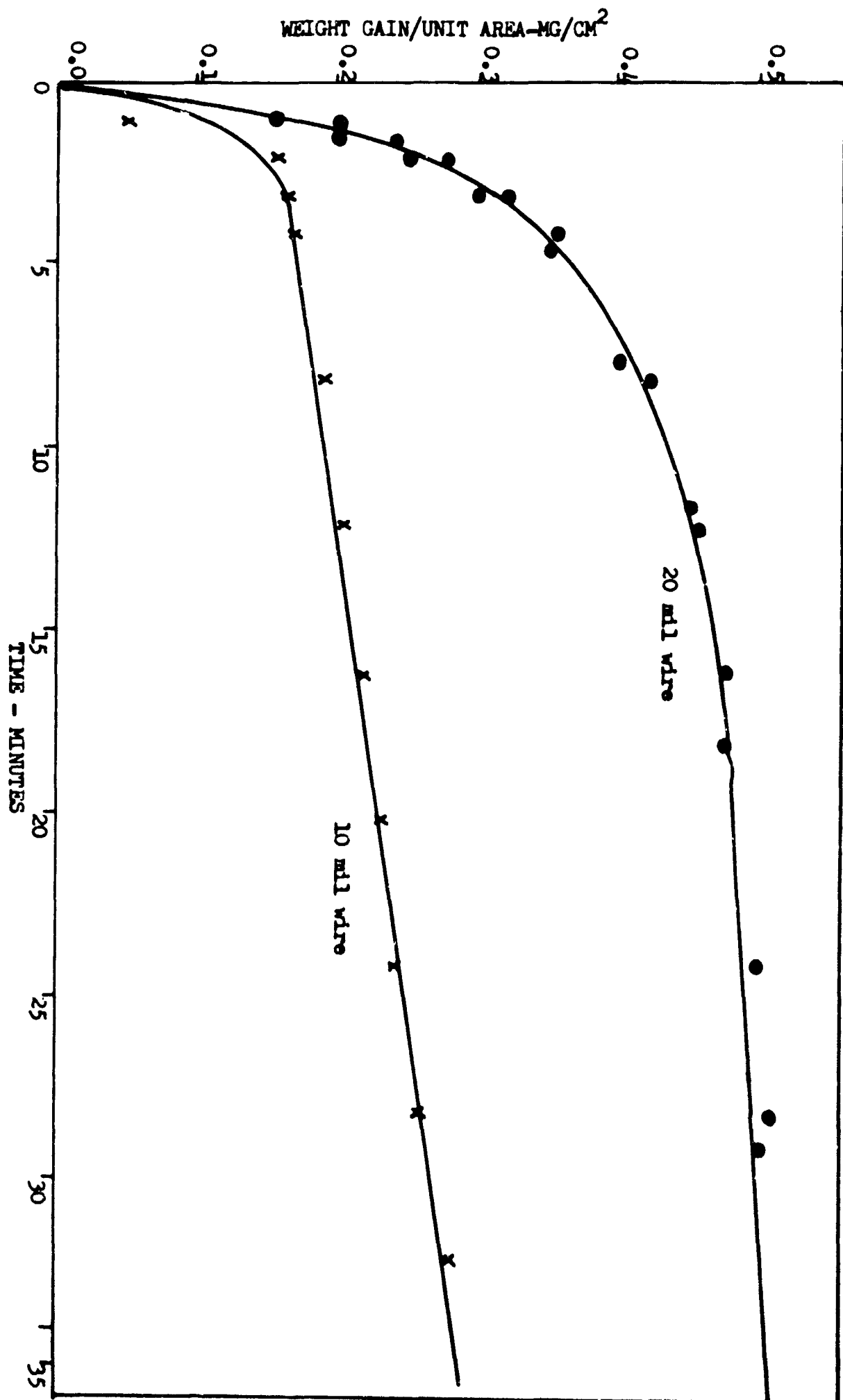
FIG. 15 EARLY OXIDATION DATA FOR RENE 41 WIRES AT 1700 F

relatively infinite thickness and corresponding infinite aluminum source never experiences the high concentration gradients as in the wires. For this reason, parabolic behavior with the resulting lower initial weight gain seen in Figs. 8 and 9 should be anticipated. Further justification for the low initial weight gain for sheet versus wire may be seen by comparing Figs. 16A and 16B. It will be noted that grain size in the sheet is much larger than in the wire. With highly active aluminum diffusing along grain boundaries, the path leading to oxidation offers much less resistance in the wires (Ref 18:411). The solutions of the differential equations for diffusion (Ref 7:441-450, 6:42-97) also satisfy these conclusions.

Metallography. Metallographic examination of exposed Rene 41 was performed in an attempt to correlate weight-gain data with depth of the alloy depleted zone. Fig. 17 shows qualitatively the increase in depth of this zone as a function of time at isothermal conditions. Examination of these photographs shows an area near the surface which appears to be free of alloying elements. This is the zone from which the majority of aluminum available for formation of Al_2O_3 has come. Average measurements of this depletion depth versus time at 1700 F are plotted in Fig. 18. These points are compared with the slope of 1700 F weight gain data showing that weight changes can be related to metal ion movement from this zone. Measurements of alloy-depletion zone depth at other times and temperatures showed the same general trends. Wlodek (Ref 52:19) summarized in his oxidation studies of Rene sheet that the movement of ions through the alloy-depleted zone is a complex phenomenon involving not only diffusion of aluminum and chromium ions outward, but also the back-diffusion of oxygen, which combines with aluminum to form a subscale of Al_2O_3. Similar internal oxidation was noted (Fig. 19) by this author while examining unetched Rene 41 wire. Measurement of the depth of oxide penetration was not performed; however, examination of the unetched specimens verified qualitatively that internal oxidation
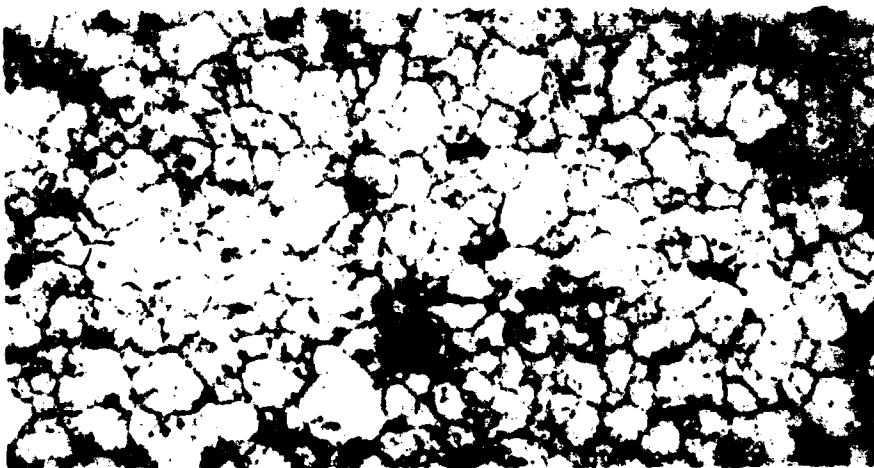
Rene 41 20 mil wire
Mag. 500 X

A.
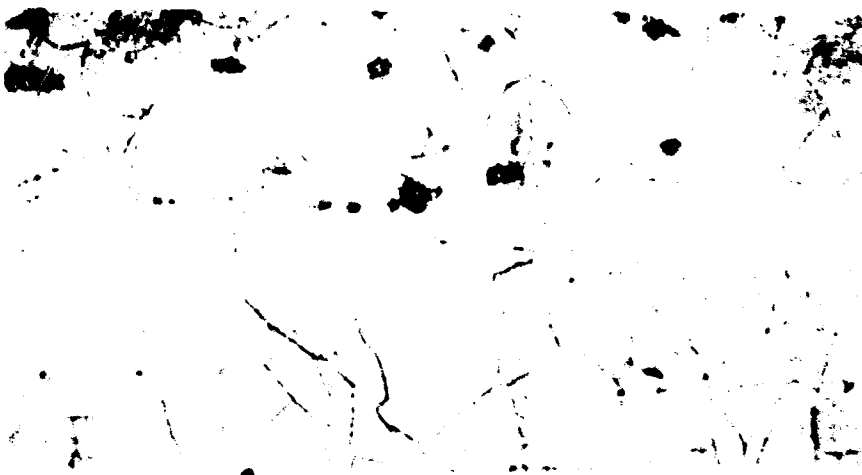
Rene 41 50 mil sheet
Mag. 500 X

B.

Fig. 16
Comparison Between Rene 41 Wire
and Sheet Grain Size

Rene 41   20 mil wire   Time: 45 minutes
Mag. 500 X
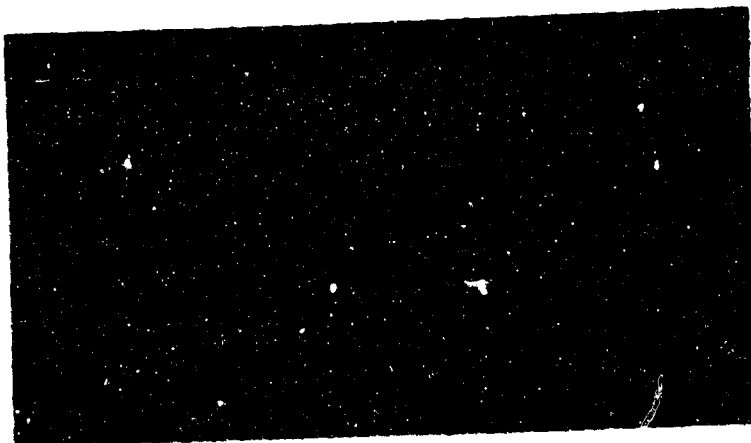
Rene 41   20 mil wire   Time: 500 minutes
Mag. 500 X
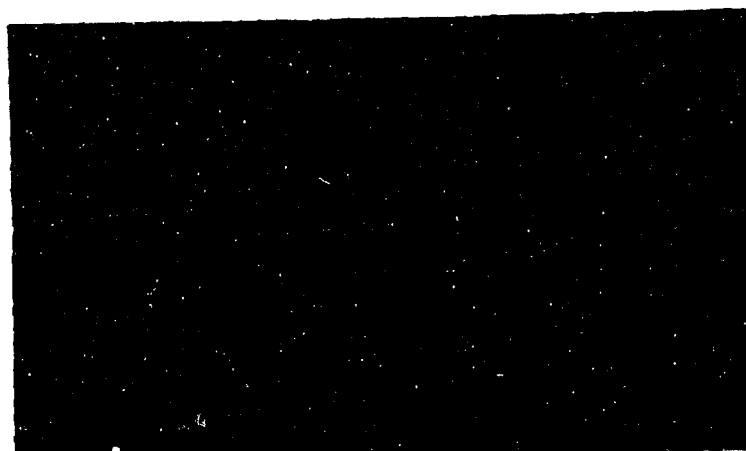
Rene 41   20 mil wire   Time: 950 minutes
Mag. 500 X

Fig. 17   Increase in Depth of Alloy Depleted Zone

in Rene 41 with Exposure Time at 1700 F

46

BLANK PAGE
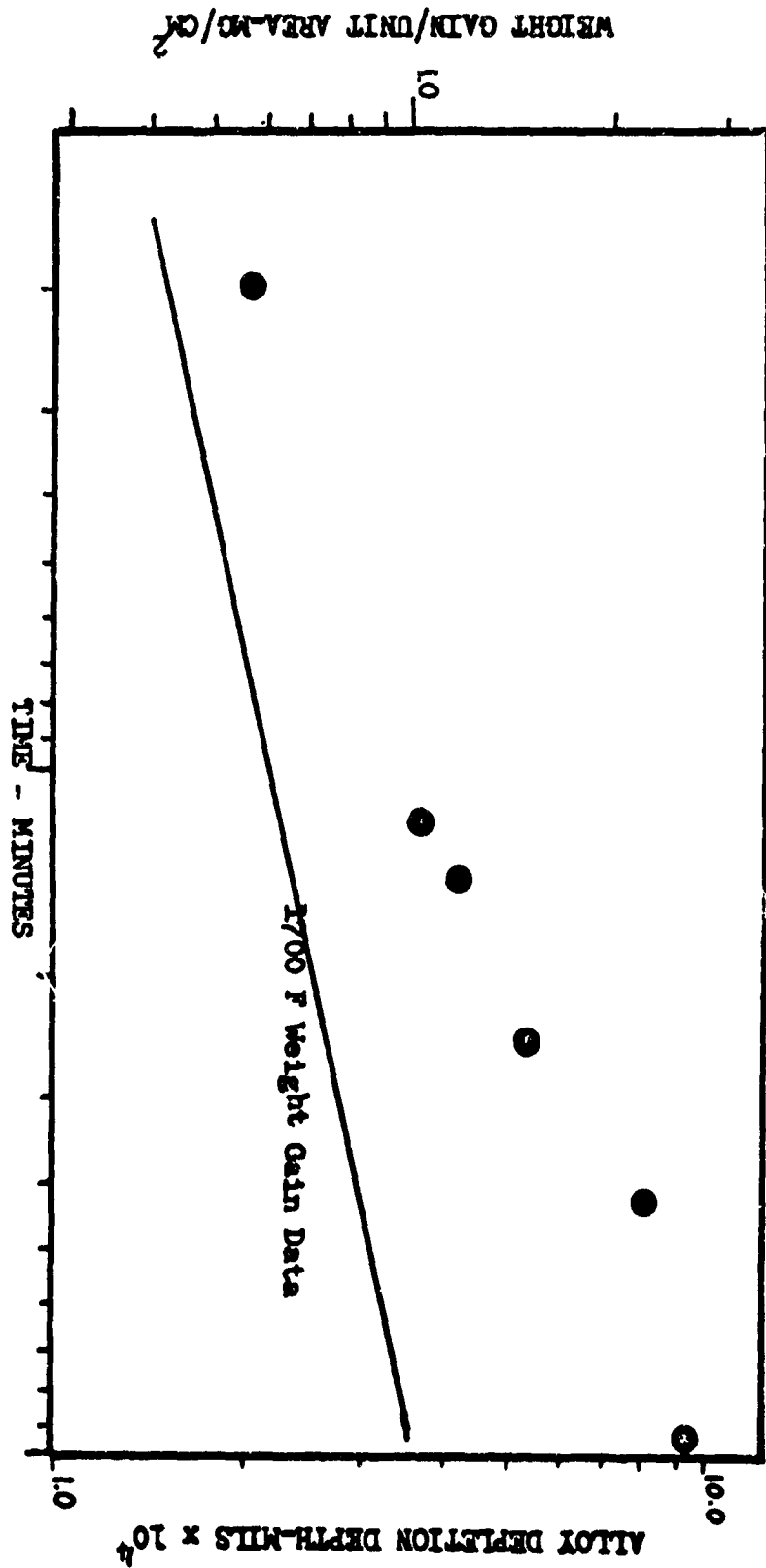
FIG.18 DEPTH OF ALLOY DEPLETION VS. TIME FOR RENE 41 AT 1700 F (20 mil wire)

Rene 41   20 mil wire   Time: 45 minutes
Mag. 1500 X   Unetched

Rene 41   20 mil wire   Time: 150 minutes
Mag. 1500 X   Unetched

Fig. 19
Increase in Depth of Internal Oxidation
with Time at 1700 F

depth and concentration increase with time. All metallographic exam-
ination of specimens could be correlated to weight-gain data.

Oxygen Partial Pressure Tests. As expected (Ref 17:396, 1:185,
33:129), exposure to different oxygen partial pressures at one
atmosphere total pressure showed no measurable effect on the rate of
oxidation of Rene 41 (Fig. 20), in that the rate controlling mechanism
appears to be diffusion of metal ions to the oxide-gas interface. As
long as a thin layer of oxygen molecules is present at that interface,
no change in rate will be observed by increasing the oxygen content.
It is believed that at extremely low oxygen partial pressures, some
effect will be noted, as presence of oxygen for combustion will then
be rate controlling.

Stress-Oxidation Testing. Oxidation tests under stress at 1600 F,
1700 F, and 2000 F revealed some effect of stress on the oxidation
rates of Rene 41. Fig. 21 compares the data for no load conditions
with stressed wires. Although data scatter reveals no measurable rates
caused by differences in stress levels, there is a definite increase
in oxidation with the application of stress. This can be attributed
to the fact that any oxide formed on a stressed specimen will begin
to crack as creep in the metal begins to occur (Ref 33:31). This
shortens the critical path for diffusion through the reaction zone,
increasing oxidation. Additionally, since loads were periodically
removed for specimen weighing, cyclic stresses could create cracks
in the oxide, further increasing weight gain.

Effect of Thermal Cycling. Comparison of oxidation results from
thermobalance, or continuous exposure testing versus cyclic exposure
to test temperatures is shown in Fig. 22 for 10 mil wire and Fig. 23
for 20 mil wire. These curves show that higher weight gain occurred
when the wires were periodically removed from the furnace for weighing.
This increase in rate can be attributed to unequal thermal gradients
in oxide and metal while cooling, which create cracks in the oxide.

WEIGHT GAIN/UNIT AREA-MG/CM^2

0.1

1.0

TIME - MINUTES

100

1000

NOTE:

X   22 % O_2

O   5 % O_2

20 mil wire

P = 1 atmosphere
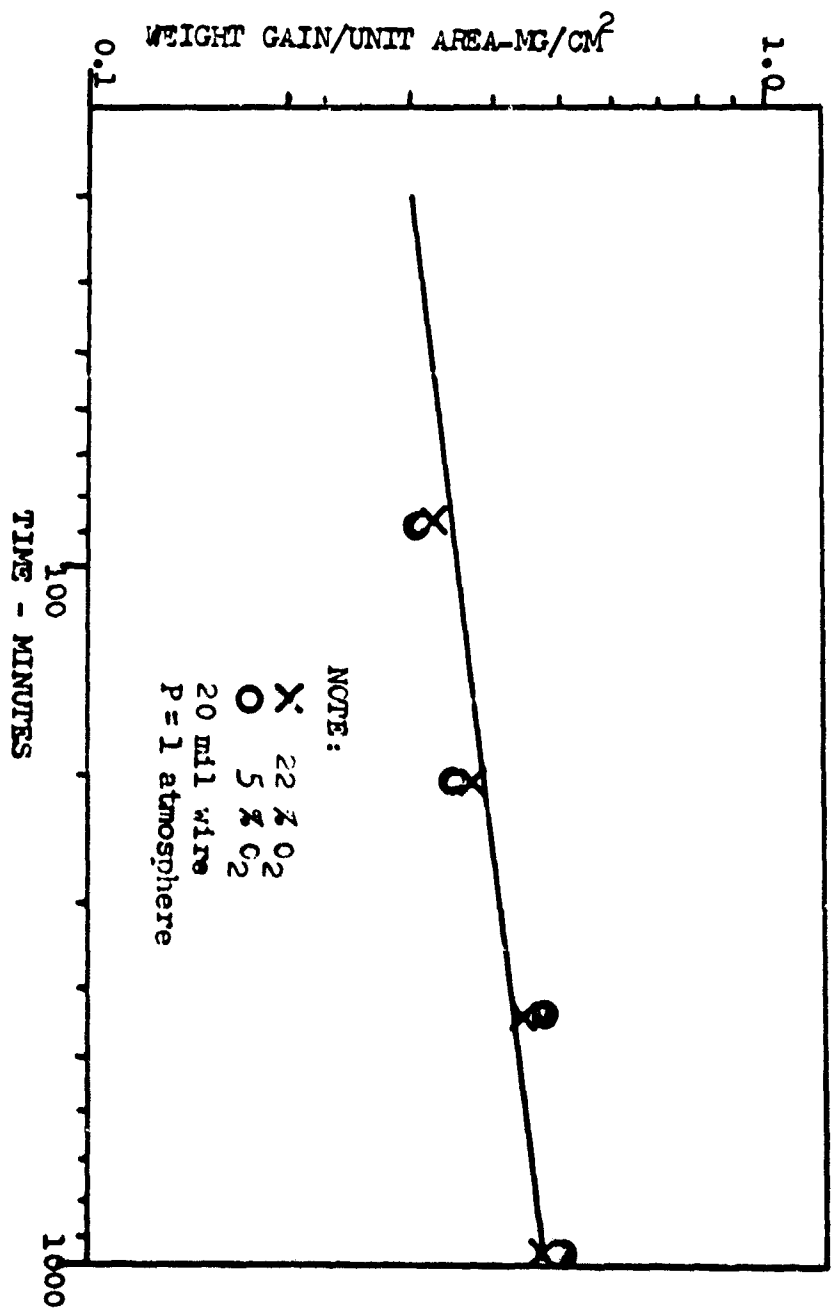
FIG. 20

EFFECT OF O_2 PARTIAL PRESSURE ON OXIDATION OF R-41 AT 1600 F
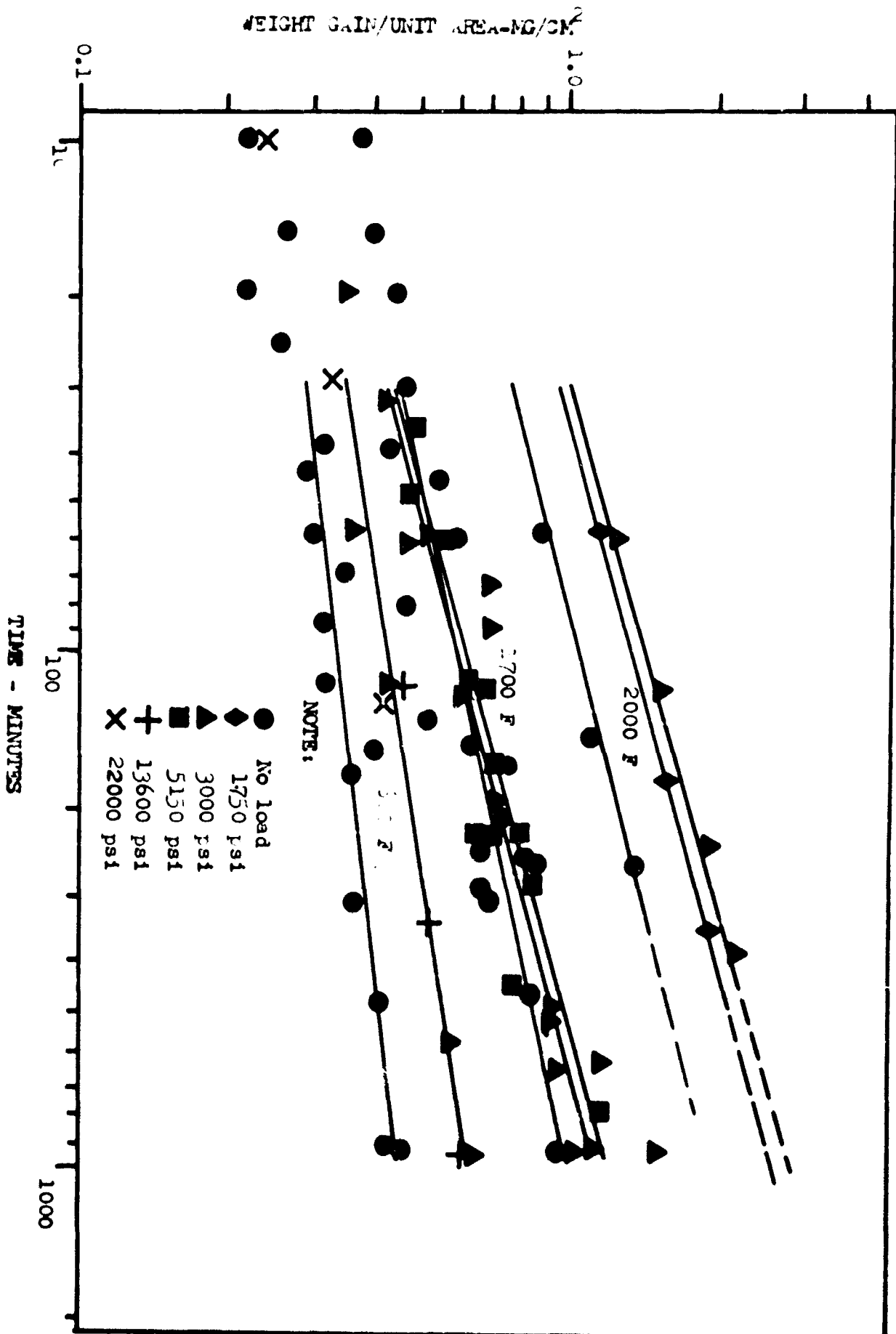
FIG. 21 EFFECT OF STRESS ON OXIDATION OF RENE 41 WIRE
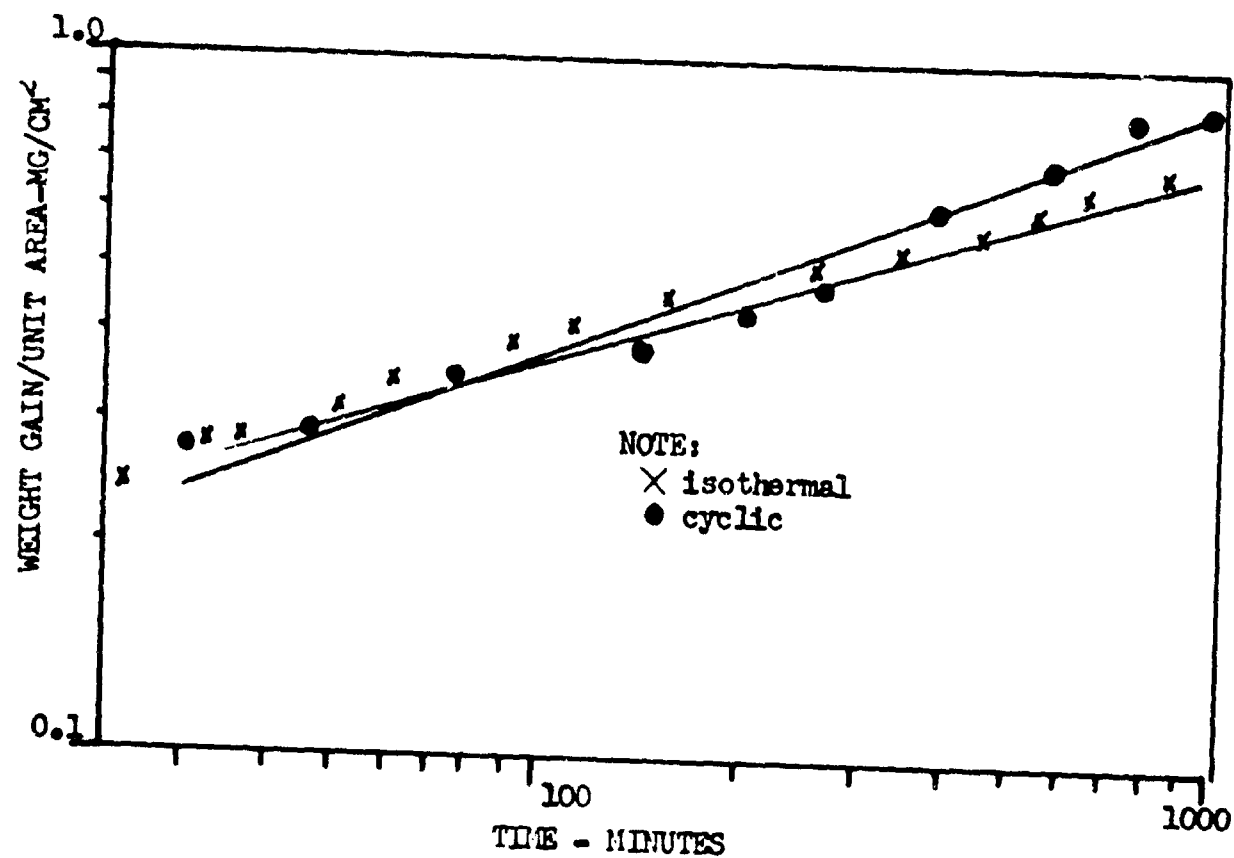
FIG. 22 COMPARISON BETWEEN ISOTHERMAL AND CYCLIC EXPOSURE
OXIDATION RATES FOR RENE 41 AT 1700 F   (10 mil wire)
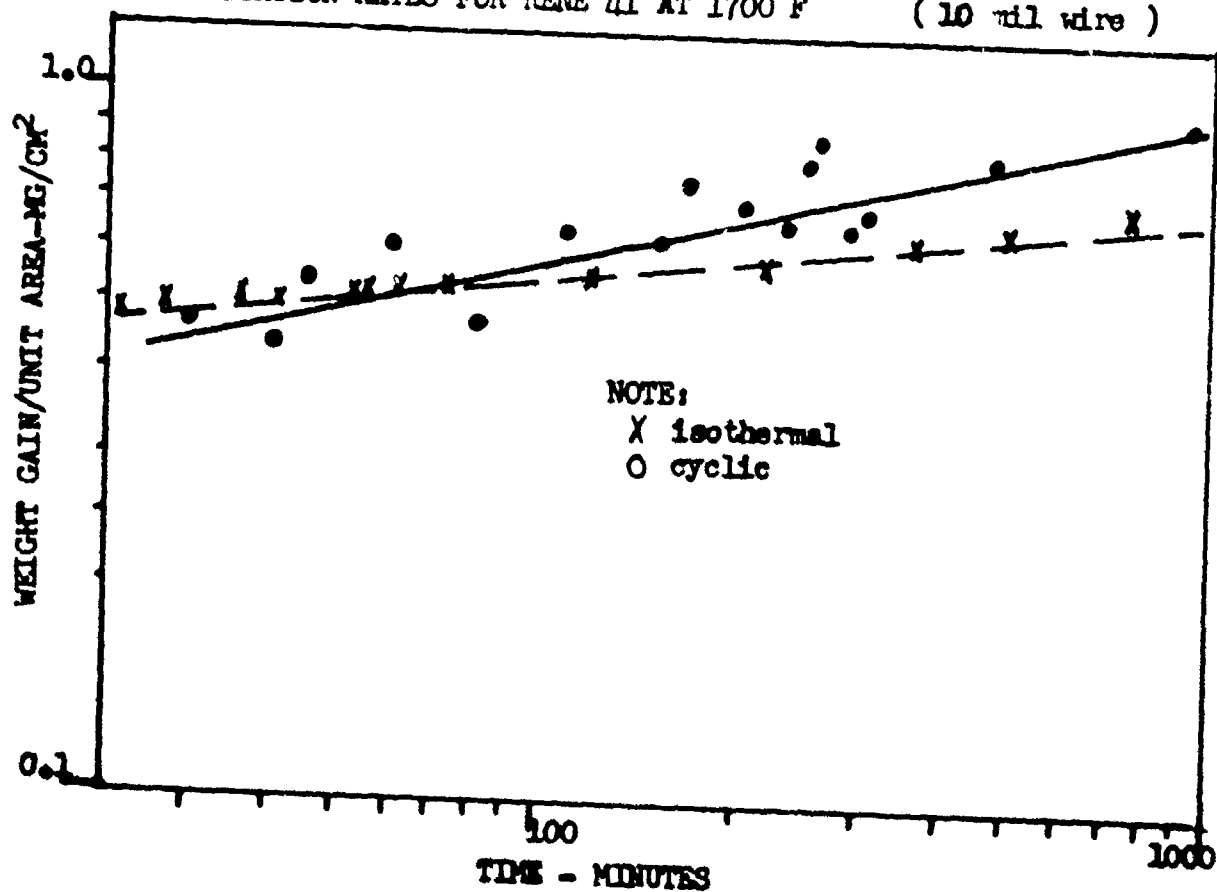
FIG. 23 COMPARISON BETWEEN ISOTHERMAL AND CYCLIC EXPOSURE
OXIDATION RATES FOR RENE 41 AT 1700 F   (20 mil wire)

These cracks which cause an increase in weight change, will heal as new oxide forms over them on further exposure to temperature.

Activation Energy. Although it has been demonstrated that oxidation in Rene 41 is a complex process influenced by geometry as well as electrochemical reactions, a semi-quantitative value of activation energy for no-load tests, using Arrhenius' equation, Eq (9), has been computed as 45 to 55 kcal/mole for sheet and wire, between 1700 F and 2000 F. Wlodek (Ref 51; Fig. 7) attributes an activation energy of 66 kcal/mole for Rene 41 sheet oxidation, while Gulbransen and Andrew (Ref 14:163) reported $Q = 38$ to 52 kcal/mole for Nichrome alloys. The differences in Wlodek's values from wire data can be attributed to the lack of parabolic kinetics in the oxidation of wires.

Summary. The oxidation of Rene 41 wire can be summarized as a process commencing with the rapid formation of a thin film of Al_2O_3. This film results from depletion of aluminum in the region immediately adjacent to the metal-oxide interface. The rate of formation of Al_2O_3 will be dependent on the concentration gradient of aluminum in the base metal; this gradient being most severe in the smaller diameter wire. Oxidation proceeds by diffusion of chromium ions along grain boundaries and through the Al_2O_3 scale. The rate of diffusion of chromium will be dependent on the simultaneous rate of increase in thickness of the Al_2O_3 scale. Internal oxidation then occurs through back-diffusion of oxygen through the alloy depleted zone, resulting in formation of Al_2O_3. Concurrently with the diffusion of chromium, but at a slower rate, nickel ions diffuse to the oxide-gas interface, leading to the growth of $NiCr_2O_4$. As weight-gain increases, this scale becomes mechanically unstable, resulting in cracking and spalling (Ref 52:19-20).

Thoriated Nickel Wire Oxidation

No-Load Testing. TD Nickel wire, composed of a high-purity nickel matrix with uniformly dispersed ThO_2 particles, was not influenced by rapid oxidation of the highly active alloying elements found in Rene 41; therefore, the analysis of the oxidation mechanisms and the determination of the rate controlling process in TD Nickel was a much simpler task than the analysis for Rene 41. Figs. 24 and 25, representing the oxidation data for 10 mil and 20 mil wire, both show near parabolic oxidation rates, indicating that diffusion of nickel and/or oxygen are the rate controlling processes.

Comparison With Other Results. An attempt was made to compare test data with the results of other investigations of high-purity nickel oxidation. The results of the comparison are given in Fig. 26, showing oxidation data for various grades of high-purity nickel. Sartell and Li (Ref 41:92), Gulbransen and Andrew (Ref 15:451) and Faust (Ref 11), in their examination of nickel, and Wlodek (Ref 50:1) and du Pont (Ref 36) testing TD Nickel, all measured parabolic rates except that Wlodek noted a quartic rate for 1600 F and early 1800 F data. Activation energies for the data presented in Fig. 26 range from 39 kcal/mole found by du Pont to 68 kcal/mole calculated by Gulbransen and Andrew. Kubaschewski and Hopkins (Ref 24:163) list Q as 38.4 kcal/mole for 99.8% purity nickel and 45 kcal/mole for 99.7% purity. Ignatov and Shamgunova (Ref 21:25) summarize the results of other investigations, stating that the activation energy for nickel ranges from 43.5 to 55 kcal/mole. An activation energy based on values of k for 10 mil data between 1600 F and 2000 F, was calculated as 42.5 kcal/mole. Discussions concerning the scatter of the curves in Fig. 26 with Mr. Paul Faust of the Electrochemical Section, Materials Testing Laboratory, Wright-Patterson AFB, have led this author to the conclusion that very small amounts of impurities in nickel may have an appreciable effect on the oxidation rates measured. Kubaschewski and Hopkins
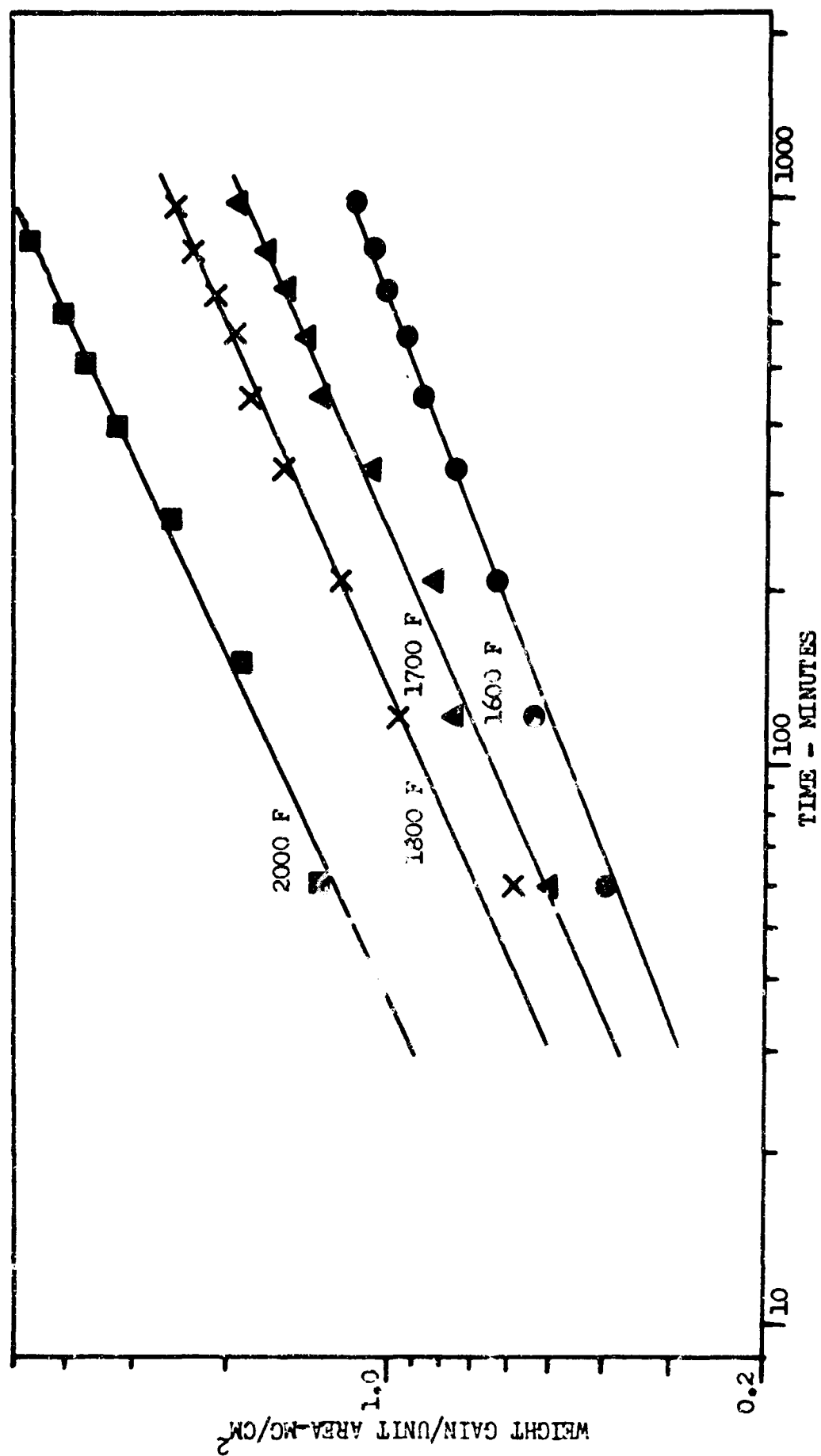
FIG. 24 OXIDATION DATA FOR T D NICKEL (10 mil wire)

55
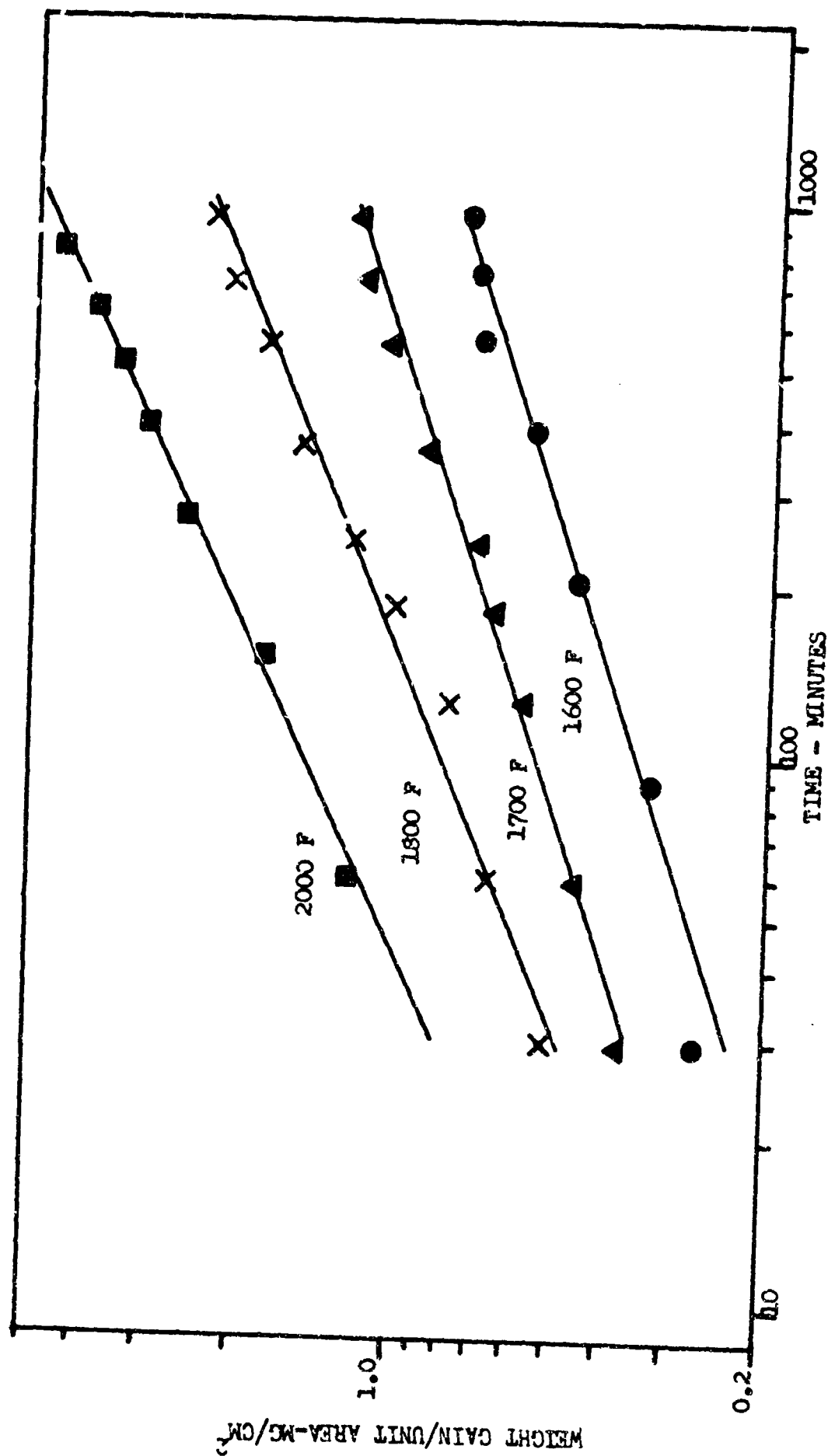
FIG. 25 OXIDATION DATA FOR T D NICKEL (20 mil wire)

TIME — MINUTES

WEIGHT GAIN/UNIT AREA-MG/CM²

2000 F

1800 F

1700 F

1600 F

56
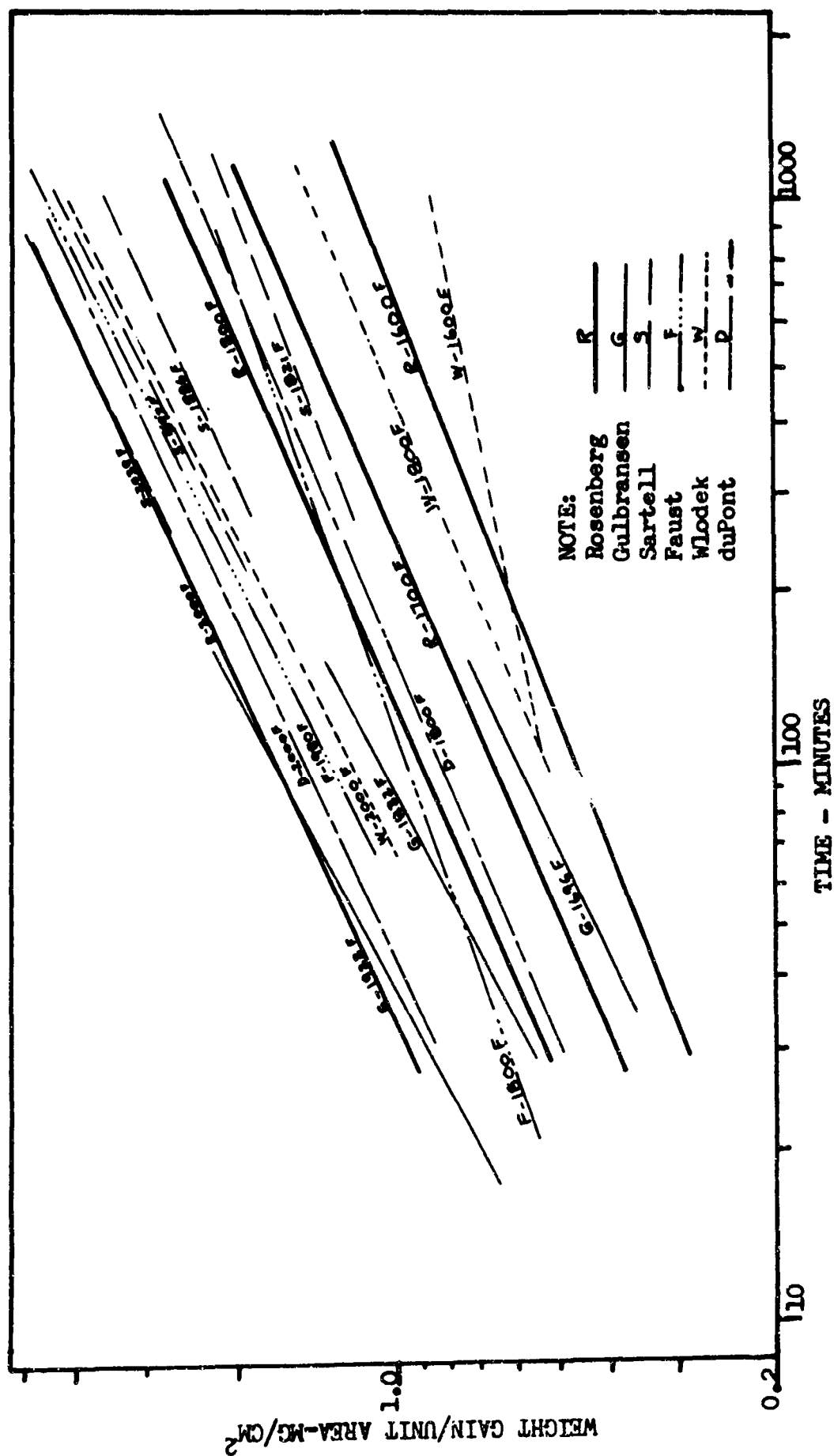
FIG. 26 COMPARISON OF SOME OXIDATION DATA ON HIGH PURITY NICKEL

57

(Ref 24:177) mention the same possibility.

Oxidation data from E. I. du Pont de Nemours and Co., developers of TD Nickel (Ref 36), compares quite favorably (see Fig. 27) with this investigation at 1800 F and 2000 F.* No lower temperature data from du Pont was available for comparison.

Oxygen Partial Pressure Tests. The results of a test at 1600 F to determine the effect, if any, of variation in O_2 partial pressure on the oxidation rates of TD Nickel is shown in Fig. 28. Measurements at 22‰ and 5‰ O_2 reveal no noticable influence of changes in oxygen content, similar to the results obtained for Rene 41.

Stress-Oxidation Testing. TD Nickel specimens under stress showed no measurable differences in oxidation rates from "no-load" conditions. A graph of weight gain per unit area versus time, Fig. 29, shows data for various stresses plotted along the "no-load" curve, with little or no deviation of stress data points from this curve. This relative insensitivity of TD Nickel oxidation to stress can be attributed to the high strength and ductility of the oxide coating (Ref 50:1, 10-11; 41:96).

Metallography. During oxidation, a green scale, NiO, was formed on the surface of the wires. Fig. 30 shows the thickness of this scale at temperatures from 1600 F to 2000 F. Unlike Rene 41 oxide, which tended to spall before 16 hours exposure at 2000 F, NiO was found to be extremely adherent, failing to crack even when the wire was twisted. Note from Fig. 30 that there appears to be no sub-scale, or internal oxidation in the TD Nickel, such as that found in metallographic examination of Rene 41. Comparisons between measured thickness of the oxide and weight-gain data showed reasonable correlation.

---

* These curves were drawn from values of k , the rate constant, given in $(mg/cm^2)^2/hour$.
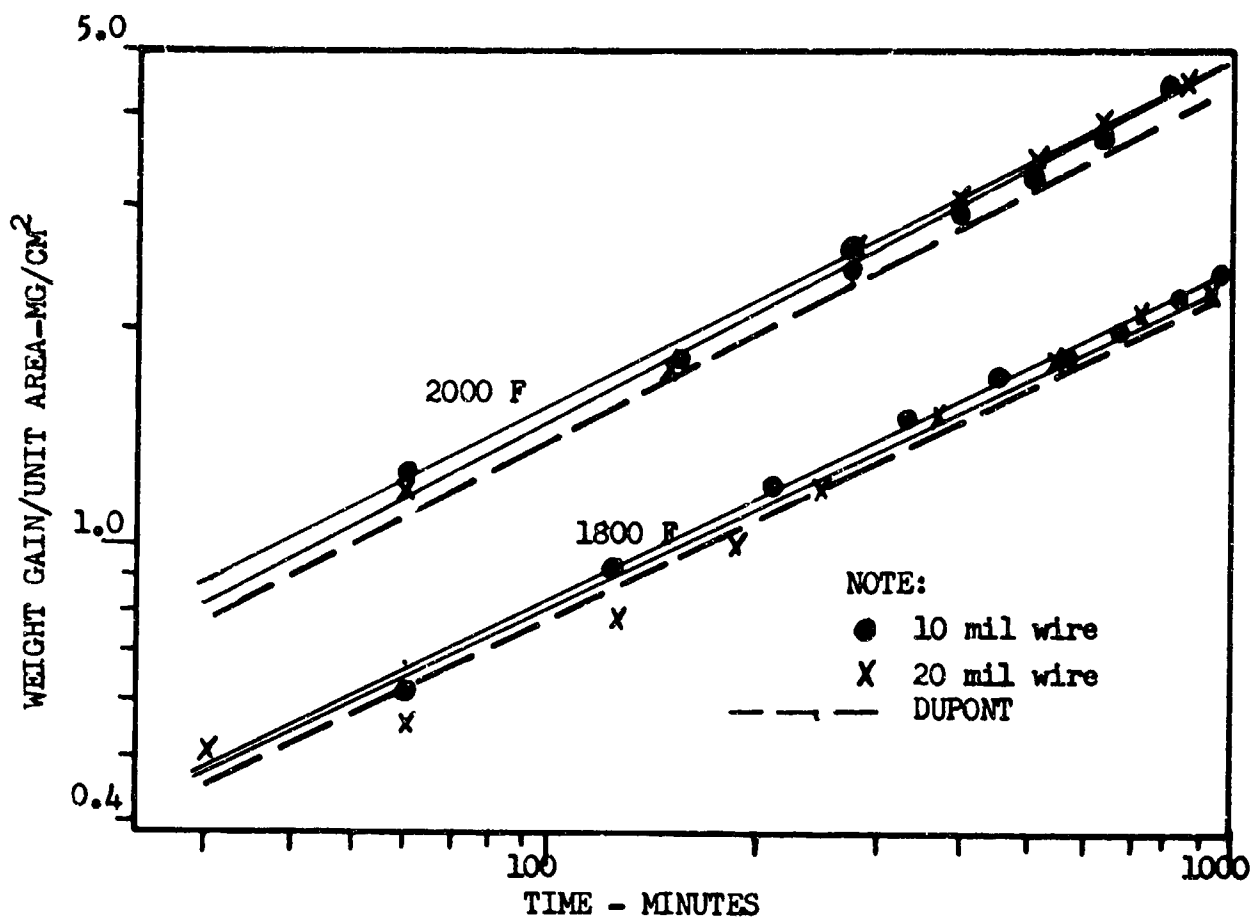
FIG.27 COMPARISON OF T D NICKEL OXIDATION DATA
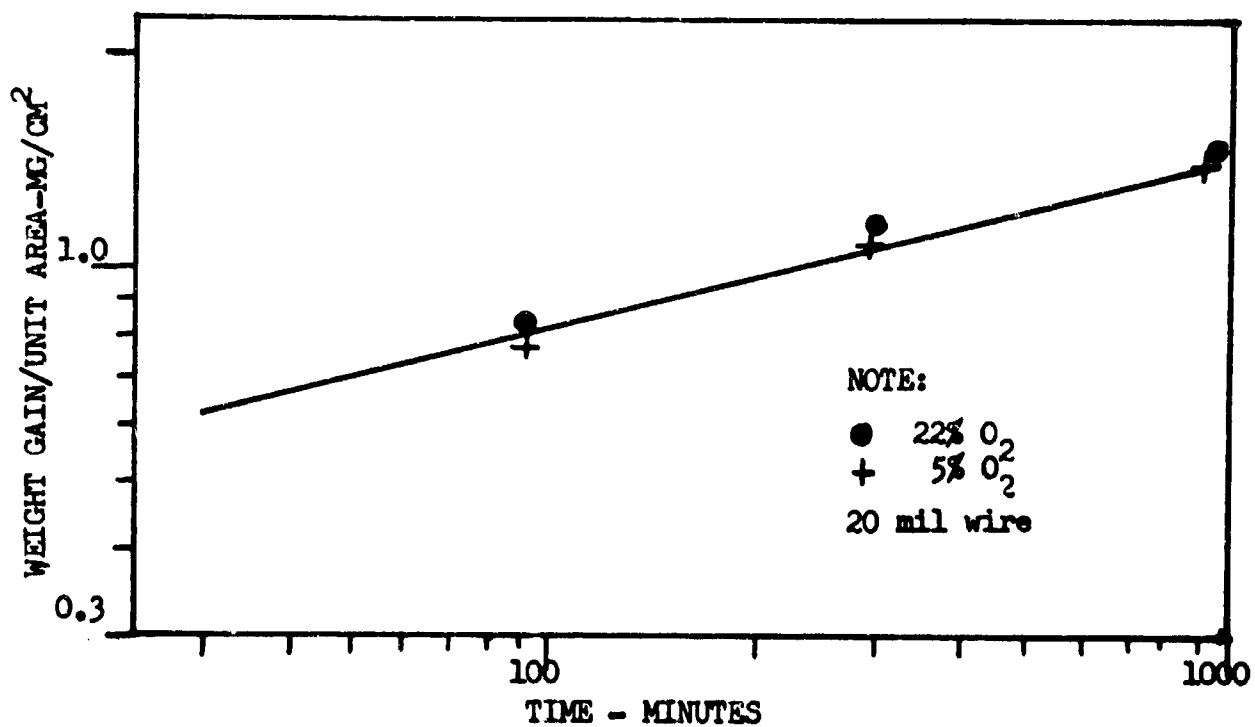
FIG.28 EFFECT OF O_2 PARTIAL PRESSURE ON OXIDATION OF T D NICKEL AT 1600 F

59
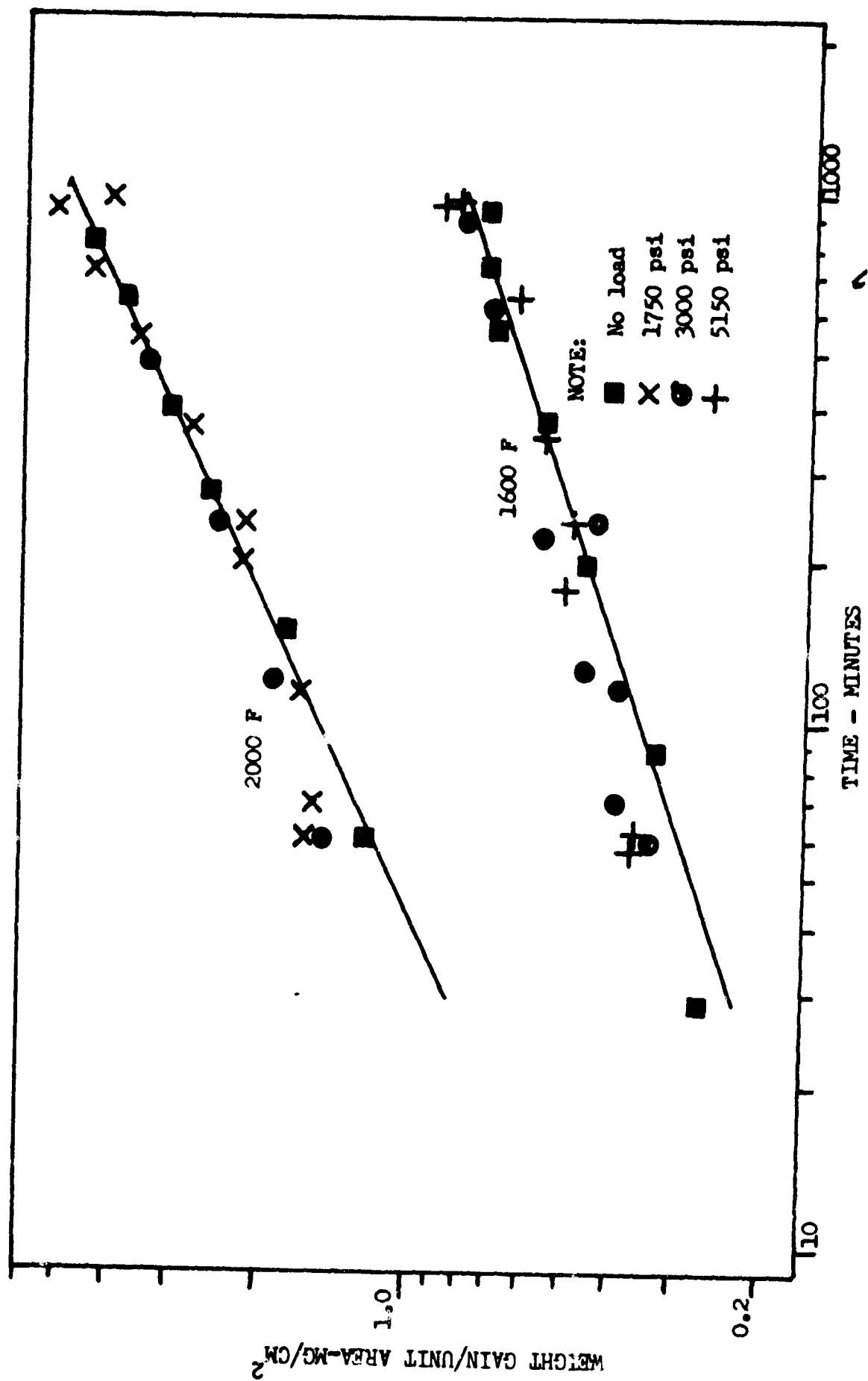
FIG. 29 EFFECT OF STRESS ON OXIDATION OF T D NICKEL (20 mil wire)
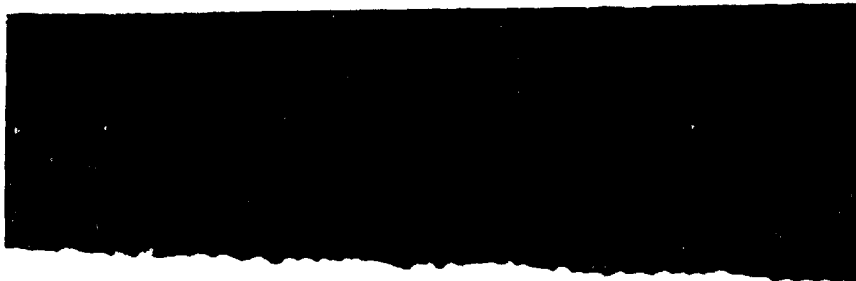
60

TD Nickel   20 mil wire   1600 F
Mag. 750 X   Unetched

TD Nickel   20 mil wire   1800 F
Mag. 750 X   Unetched

TD Nickel   20 mil wire   2000 F
Mag. 750 X   Unetched

Fig. 30
Variation in NiO Thickness on TD Nickel
with Temperature at 960 minutes

Summary. TD Nickel wire oxidation can be described by the laws for parabolic kinetics. The rate controlling process has been described as a combination of diffusion of nickel ions outward and oxygen ions inward through the oxide by previous investigations of high-purity nickel, and is summarized on page 17 of this thesis.

V. Conclusions and Recommendations

Rene 41 wire oxidation is a complex reaction controlled by several mechanisms and factors, which may be summarized as a process commencing with asymptotic growth of Al_2O_3. This is followed by linear then parabolic diffusion of chromium ions to form Cr_2O_3. Later, overgrowth of $NiCr_2O_4$ and NiO occurs, resulting in an unstable oxide which spalls easily. The initial diffusion of aluminum influences the later formation of Cr_2O_3 in proportion to the thickness of the Al_2O_3 layer.

The thickness of the Al_2O_3 layer on Rene 41 will be dependent on the concentration gradient of aluminum across the specimen. This concentration gradient is more severe in wire than in thick sheet material, where an infinitely deep source of aluminum is present for diffusion.

Reduction in load-bearing cross-sectional area and brittleness will be caused by internal oxidation in Rene 41 at long exposure times and high temperatures; therefore, for practical, long term uses of Rene 41 wire, protective coatings should be applied to the metal surface to reduce the detrimental effects of internal oxidation.

TD Nickel wire oxidation, by comparison with Rene 41, is a simple, parabolic process involving the growth of NiO scale on the surface of the metal. Although weight-gain from oxidation is relatively high, internal oxidation is non-existant, with the result that the metal remains ductile and retains much of its strength after high temperature exposure.

The author recommends that high-temperature oxidation tests on other Ni-Cr-Ti-Al alloy wires be performed in order to further ascertain the validity of the theory presented in this investigation. It is suggested that these studies be limited to shorter duration test periods, and that several wire diameters be selected for testing so that definite trends may be established.

It is recommended that further stress-oxidation testing of Ni-Cr superalloys be performed to determine their susceptibility to mechanical deterioration caused by oxide formation.

Bibliography

1. Baur, J. P., et al. "High Pressure Oxidation of Metals, Nickel in Oxygen." Journal of the Electrochemical Society, 110:185 (March 1963).

2. Blum, B. S. Determination of Causes of Cracking in Welding Age Hardenable High Temperature Alloys. ASD Technical Report 61-678. Wright-Patterson AFB, Ohio: Aeronautical Systems Division, November, 1961.

3. Borgmann, C. W., et al. Corrosion of Metals. Cleveland: American Society for Metals, 1946.

4. Brasunas, A. S., et al. Symposium on Corrosion Fundamentals. Knoxville: University of Tennessee Press, 1956.

5. Clark, F. H. Metals at High Temperatures. New York: Reinhold Co., 1950.

6. Crank, J. The Mathematics of Diffusion. London: Oxford University Press, 1956.

7. Darken, L. S., and Gurry, R. W. Physical Chemistry of Metals. New York: McGraw-Hill Book Co., Inc., 1953.

8. Dunn, J. S. "Oxidation of Tungsten." Journal of the Chemical Society, I:1149-1150 (1929).

9. "Dynamics and Structures" Space Aeronautics, 40:39-50 (July 1963).

10. Evans, U. R. Metallic Corrosion, Passivity and Protection. New York: Longmans, Green and Co., 1948.

11. Faust, Paul R. High Purity Nickel. Unpublished Oxidation Test Data. Materials Central, Wright-Patterson AFB, Ohio. April 1964.

12. Favor, R. J., et al. Design Information on Nickel-Base Alloys for Aircraft and Missiles. DMIC Report 132. Columbus, Ohio: Defense Metals Information Center, 1960.

13. Fishmeister, H. F. Reactivity of Solids, edited by J. H. de Boer, New York: Elsevier Publishing Co., 1961, p 195.

14. Gulbransen, E. A., and Andrew, K. F. "Rate of Oxidation of Three Ni-Cr Heater Alloys between 500-900 C." _Journal of the Electrochemical Society_, 101:163 (April 1954).

15. ----. "High Temperature Oxidation of High Purity Nickel between 750-1050 C." _Journal of the Electrochemical Society_, 104:451-454 (July 1957).

16. ----. "The Kinetics of Oxidation of High Purity Nickel." _Journal of the Electrochemical Society_, 101:128 (March 1954).

17. ----. "The Kinetics of the Reactions of Vanadium with Oxygen and Nitrogen." _Journal of the Electrochemical Society_, 97:396 (November 1950).

18. Guy, A. G. _Elements of Physical Metallurgy_. Reading, Mass: Addison-Wesley Publishing Co., Inc., 1960.

19. Heldenfels, R. R. "Structures and Materials." _Astronautics and Aerospace Engineering_, 1:75 (November 1963).

20. Hoag, J. C. The Evolution of Nickel-Base Precipitation-Hardening _Superalloys_. DMIC Memorandum 84. Columbus, Ohio: Defense Metals Information Center, 1961.

21. Ignatov, D. V., and Shamgunova, R. D. _Mechanism of the Oxidation of Nickel and Chromium Alloys_. NASA Technical Translation F-59. Washington: National Aeronautics and Space Administration, 1961.

22. Johnson, D. E., et al. _Candidate Materials for High Temperature Fabrics_. ASD Technical Report 59155. Wright-Patterson AFB, Ohio: Aeronautical Systems Division, September 1959.

23. ----. _Metal Filaments for High Temperature Fabrics_. ASD Technical Report 62-180. Wright-Patterson AFB, Ohio: Aeronautical Systems Division, February 1962.

24. Kubaschewski, O., and Hopkins, B. E. _Oxidation of Metals and Alloys_. New York: Academic Press Inc., 1953.

25. Lipka, J. _Graphical and Mechanical Computation_. New York: John Wiley and Sons, 1946.

26. Mallett, M. W. "Purification of Argon." _Industrial and Engineering Chemistry_, 42:2095-2096 (November 1950).

27. Manning, C. R., et al. An Investigation of a New Nickel Alloy Strengthened by Dispersed Thoria. NASA Technical Notice D-1944. Washington: National Aeronautics and Space Administration, July 1963.

28. Maron, S. H., and Prutton, C. F. Principles of Physical Chemistry. New York: MacMillan Company, 1961.

29. Miley, H. A. "Fundamentals of Oxidation and Tarnish," in Corrosion Handbook, edited by H. H. Uhlig. New York: John Wiley and Sons, 1948.

30. Morris, R. J. "Rene 41...New Higher-Strength Nickel Base-Alloy." Metal Progress, 76:67 (December 1959).

31. Oxidation of Experimental Alloys, Part II--Nickel-Molybdenum Alloy. National Bureau of Standards Report 5899, Washington: GPO, n.d.

32. Oxidation of Materials at High Temperatures. NAA Report AL-2618. North American Aviation, Inc., 13 September 1957.

33. Parker, E. R., et al. High Temperature Properties of Metals. Cleveland: American Society for Metals, 1951.

34. Pessl, H. J. Evaluation of Iron and Nickel-Base Alloys for Medium and High Temperature Reactor Applications, Part I. AEC Research and Development Report. Washington: Atomic Energy Commission, February 1961.

35. Pollock, W. I. Research Supervisor, Metal Products, E. I. du Pont de Nemours and Co., Wilmington, Delaware. Private communication to Capt. R. A. Rosenberg, AFIT (September 1963).

36. -----. Private Communication, with TD Nickel Oxidation Data enclosure to Prof. J. R. Myers, AFIT (April 1963).

37. Rhines, F. N. Effect of the Mechanical Behavior of Oxidation Products on the Scaling of Columbium and Columbium-Rich Alloys. Research Proposal. Gainesville, Florida: University of Florida, January 1963.

38. Rhines, F. N., et al. "Rates of High Temperature Oxidation of Dilute Copper Alloys." Transactions of AIME, 147:205 (1942).

39. Richmond, J. C., and Thornton, H. R. Oxidation of Experimental Alloys, Part II. ASD Technical Report 58-164. Wright-Patterson AFB, Ohio: Aeronautical Systems Division, February 1959.

40. Sansom, F. J. *Thermal Stresses in Infinite Cylinders.* ASNCC Internal Memorandum 62-28. Wright-Patterson AFB, Ohio: Aeronautical Systems Division, September 1962.

41. Sartell, J. A., and Li, C. H. "Mechanism of Oxidation of High-Purity Nickel in the Range 950-1200 C." *Journal of the Institute of Metals,* 90:92-96 (November 1961).

42. Siebert, C. A., et al. *An Investigation of Intergranular Oxidation in Stainless Steels and High Nickel Alloys.* ASD Technical Report 55-470. Wright-Patterson AFB, Ohio: Aeronautical Systems Division, October 1956.

43. Smith, G. V. *Properties of Metals at Elevated Temperatures.* New York: McGraw Hill, 1950.

44. Stuart, R. E., and Starr, C. D. "New Design Data on TD Nickel." News Bulletin reprinted from *Materials in Design Engineering* (August 1963), New York: Reinhold Co., 1963.

45. *Study of a Drag Brake Satellite Recovery System.* ASD Technical Report 61-348. Wright-Patterson AFB, Ohio: Aeronautical Systems Division, January, 1962.

46. Titus, G. W., and Brunhouse, J. S. "Long Term Air Corrosion of Several Nickel-Based Alloys." *Corrosion,* 19:339 (October 1963).

47. Uhlig, H. H. *Corrosion and Corrosion Control.* New York: John Wiley and Sons, Inc., 1963.

48. ----. "Effect of Metal Composition and Structure on Corrosion and Oxidation." *Corrosion,* 19 (July 1963).

49. Wadsworth, M. *Physical Chemistry of Hydrometallurgy, Chapter 3.* Lecture Notes. Salt Lake City: University of Utah, n.d.

50. Wlodek, S. T. *The Oxidation of Ni-2% ThO$_2$.* G. E. Technical Information Series Report. Cincinnati: General Electric Co., May 1962.

51. ----. *The Oxidation of Rene 41 and Udimet 700.* Unpublished report. Cincinnati: General Electric Co., n.d.

52. ----. *The Oxidation of R-41, U-700 and Hastelloy Alloy X.* G. E. Technical Information Series Report. Cincinnati: General Electric Co., February 1962.

53. Wolk, J. S., and Evans, E. G. "Effect of Oxygen Pressure on Internal Oxidation of Nickel-Aluminum Alloys." Corrosion, 18:129 (April 1962).

APPENDIX A

OXIDATION WEIGHT GAIN MEASUREMENTS

(Intermittent Analytical Balance Weighing)

RENE 41 50 MIL SHEET NO LOAD

1600 F		1700 F		1800 F	
Δt *	Δm **	Δt	Δm	Δt	Δm
10	.022	10	.091	10	.215
20	.110	20	.142	20	.274
25	.116	40	.160	40	.298
35	.133	80	.228	80	.376
40	.121	160	.342	160	.543
55	.145	229	.410	229	.620
80	.171	440	.558	438	.823
95	.191	740	.685	598	.942
160	.264			898	1.080
175	.289				
220	.286				
235	.312				
432	.374				
447	.405				
612	.429				
627	.457				
972	.516				
987	.495				

RENE 41 10 MIL WIRE NO LOAD

1600 F		1700 F		1800 F		2000 F	
Δt	Δm	Δt	Δm	Δt	Δm	Δt	Δm
15	.157	15	.117	15	.157	60	.783
30	.176	15	.118	45	.353	150	1.097
90	.196	30	.273	75	.490	270	1.351
210	.239	45	.294	140	.529	390	1.665
390	.314	75	.353	200	.608	510	1.743
570	.392	140	.372	260	.686	635	spalling
750	.490	200	.431	380	.902		
960	.529	260	.470	560	1.058		
		380	.608	740	1.215		
		560	.706	960	1.274		
		740	.843				
		960	.862				

* t expressed in minutes

** m expressed in mg/cm^2

70

RENE 41   20 MIL WIRE   NO LOAD

1600 F		1700 F		1800 F		2000 F	
Δt	Δm	Δt	Δm	Δt	Δm	Δt	Δm
10	.233	10	.339	10	.495	60	.890
10	.238	10	.407	10	.562	150	1.120
15	.272	10	.400	10	.577	270	1.399
20	.226	15	.409	10	.468	390	spalling
25	.267	15	.389	14	.466		
30	.297	20	.461	20	.676		
40	.321	20	.452	20	.612		
45	.300	20	.372	30	.696		
60	.306	20	.490	30	.595		
70	.358	30	.481	60	.815		
90	.332	40	.526	58	.623		
90	.367	40	.409	60	.775		
120	.340	40	.497	90	.835		
120	.362	40	.389	92	.814		
161	.401	45	.585	110	.726		
180	.369	45	.529	150	.855		
315	.374	60	.621	290	.895		
497	.416	80	.483	465	1.133		
931	.428	105	.702	649	1.173		
956	.476	106	.603	904	1.332		
		135	.467				
		135	.588				
		150	.641				
		165	.765				
		197	.715				
		235	.678				
		250	.817				
		254	.864				
		290	.661				
		303	.689				
		465	.841				
		904	.942				

RENE 41 20 MIL WIRE 1600 F (OXYGEN PARTIAL PRESSURE TEST)

5% O$_2$		22% O$_2$	
Δt	Δm	Δt	Δm
90	.327	90	.318
210	.366	210	.357
450	.454	450	.484
990	.479	990	.496

71

REME 41   20 MIL WIRE   1600 F   LOADED

3000 psi		13,600 psi		22,000 psi	
Δt	Δm	Δt	Δm	Δt	Δm
60	.377	120	.450	10	.246
120	.453	350	.527	30	.328
120	.457	1000	.641	130	.420
350	.532			130	rupture
350	.529				
585	.566				
1000	.650				

REME 41   20 MIL WIRE   1700 F   LOADED

3000 psi		5150 psi		7500 psi		13,600 psi	
Δt	Δm	Δt	Δm	Δt	Δm	Δt	Δm
33	.430	20	.360	60	.642	31	.480 rupture
60	.500	37	.486	60	.648	34	.482 • •
60	.530	50	.462	120	.718	60	.517 • •
63	.470	60	.561	120	.725	114	.700 • •
74	.700	120	.636	330	.869		
90	.700	120	.673	364	.887		
120	.610	170	.693	382	1.029		
194	.820	230	.809	382	rupture		
494	.940	240	.674				
542	.930	240	.711				
635	1.180	290	..847				
674	.970	425	.785				
955	1.520	570	.897				
960	1.160	800	1.197				
974	1.050						

REME 41   20 MIL WIRE   2000 F   LOADED

1750 psi		3000 psi	
Δt	Δm	Δt	Δm
60	1.200	60	1.208
180	1.570	120	1.510
360	1.920	245	1.980
660	spalling	390	2.220
		390	rupture

TD NICKEL   10 MIL   NO LOAD

1600 F		1700 F		1800 F		2000 F	
Δt	Δm	Δt	Δm	Δt	Δm	Δt	Δm
60	.392	60	.508	60	.685	60	1.319
120	.548	120	.762	120	.960	150	1.889
210	.627	210	.821	210	1.234	270	2.530
330	.744	330	1.055	330	1.508	390	3.172
445	.862	445	1.348	445	1.821	510	3.706
565	.920	565	1.426	565	1.919	635	4.134
685	.999	685	1.563	685	2.096	815	4.633
810	1.058	810	1.699	810	2.291		
990	1.195	990	1.954	990	2.468		

TD NICKEL   20 MIL   NO LOAD

1600 F		1700 F		1800 F		2000 F	
Δt	Δm	Δt	Δm	Δt	Δm	Δt	Δm
15	.156	30	.387	30	.530	60	1.244
30	.274	60	.484	60	.687	150	1.806
90	.333	125	.581	125	.804	270	2.588
210	.469	185	.678	185	1.040	390	3.010
390	.567	245	.716	245	1.236	510	3.571
570	.724	365	.910	365	1.569	635	3.993
750	.734	545	1.104	545	1.863	815	4.615
960	.763	725	1.220	725	2.196		
		945	1.297	945	2.373		

TD NICKEL   20 MIL   1600 F   OXYGEN PARTIAL PRESSURE TEST

5% O_2			22% O_2	
Δt	Δm		Δt	Δm
90	.792		90	.822
300	1.110		300	1.149
940	1.471		940	1.453

TD NICKEL   20 MIL   1600 F   LOADED

3000 psi

Δt	Δm
60	.362
70	.403
120	.400
125	.475
245	.450
605	.700
905	.800

5150 psi

Δt	Δm
60	.375
180	.520
360	.583
660	.673
1000	.850
60	.372
240	.500
975	.950

TD NICKEL   20 MIL   2000 F   LOADED

1750 psi

Δt	Δm
60	1.68
70	1.62
125	1.70
200	2.28
240	2.21
360	2.88
540	3.68
720	4.28
905	5.43
975	4.20

3000 psi

Δt	Δm
60	1.60
120	1.92
240	2.48
480	3.50
1000	5.05

74

(Continuous "Thermobalance" Weighing at 1700 F, No Load)

	RENE 41 10 MIL WIRE				RENE 41 20 MIL WIRE			
	RUN 1		RUN 2		RUN 1		RUN 2	
Δt	Δm	Δt	Δm	Δt	Δm	Δt	Δm
1	.050	4	.200	1	.155	1	.200
2	.160	10	.220	1.5	.200	1.5	.240
3	.165	22	.260	2	.250	2	.278
4	.172	30	.280	3	.300	3	.322
8	.192	46	.310	4.5	.350	4	.356
12	.205	62	.345	7.5	.400	8	.422
16	.216	90	.390	11.5	.450	12	.456
20	.229	110	.415	17	.473	16	.475
24	.240	150	.445	29	.500	24	.497
28	.258	246	.500	41	.510	28	.506
32	.278	342	.535	53	.520	36	.512
36	.280	438	.575	61	.530	44	.518
50	.310	534	.610			56	.522
60	.330	630	.645			72	.530
80	.355	726	.670			120	.550
156	.460	822	.700			216	.570
330	.523					360	.610
522	.579					500	.633
762	.635					750	.680
1434	.760					1000	.750
						1380	.870

APPENDIX B

Computed Values for the Solution of $\Delta m^b = kt$

RENE 41   50 MIL SHEET   NC LOAD

	b*	k**	v***
1600 F	2.28	$.252 \times 10^{-3}$	$.606 \times 10^{-2}$
1700	1.97	$.700 \times 10^{-3}$	$.143 \times 10^{-2}$
1800	2.34	$.141 \times 10^{-2}$	$.143 \times 10^{-2}$

RENE 41   10 MIL WIRE   NO LOAD

1600	3.01	$.109 \times 10^{-3}$	$.107 \times 10^{-1}$
1700	2.87	$.606 \times 10^{-3}$	$.179 \times 10^{-1}$
1800	2.36	$.189 \times 10^{-2}$	$.166 \times 10^{-1}$
2000	2.60	$.866 \times 10^{-2}$	$.675 \times 10^{-2}$

RENE 41   20 MIL WIRE   NO LOAD

1600	8.57	$.115 \times 10^{-5}$	$.519 \times 10^{-2}$
1700	4.64	$.681 \times 10^{-3}$	$.134$
1800	4.99	$.338 \times 10^{-2}$	$.556 \times 10^{-1}$
2000	3.80	$.124 \times 10^{-1}$	————

RENE 41   20 MIL WIRE   1600 F LOADED

3000 psi	5.70	$.790 \times 10^{-4}$	$.960 \times 10^{-3}$
22,000 psi	5.65	$.790 \times 10^{-4}$	————

RENE 41   20 MIL WIRE   1700 F LOADED

3000 psi	3.43	$.196 \times 10^{-2}$	$.205$
5150 psi	3.65	$.151 \times 10^{-2}$	$.566 \times 10^{-1}$
13,600 psi	4.80	$.189 \times 10^{-2}$	$.123 \times 10^{-1}$
22,000 psi	3.54	$.215 \times 10^{-2}$	$.292 \times 10^{-2}$

TD NICKEL 10 MIL WIRE NO LOAD

1600	2.63	$.148 \times 10^{-2}$	$.344 \times 10^{-2}$
1700	2.14	$.387 \times 10^{-2}$	$.267 \times 10^{-1}$
1800	2.18	$.751 \times 10^{-2}$	$.950 \times 10^{-2}$
2000	2.02	$.265 \times 10^{-1}$	$.422 \times 10^{-1}$

TD NICKEL 20 MIL WIRE NO LOAD

	b^*	k^{**}	v^{***}
1600 F	2.75	$.582 \times 10^{-2}$	$.797 \times 10^{-2}$
1700	2.75	$.210 \times 10^{-2}$	$.137 \times 10^{-1}$
1800	2.19	$.685 \times 10^{-2}$	$.441 \times 10^{-1}$
2000	1.97	$.238 \times 10^{-1}$	$.339 \times 10^{-1}$

TD NICKEL 20 MIL WIRE 1600 F LOADED

3000 psi	3.63	$.405 \times 10^{-3}$	$.117 \times 10^{-1}$
5150 psi	3.36	$.549 \times 10^{-3}$	$.229 \times 10^{-1}$

TD NICKEL 20 MIL WIRE 2000 F LOADED

1750 psi	2.40	$.399 \times 10^{-1}$	$.144 \times 10^{-1}$
3000 psi	2.42	$.442 \times 10^{-1}$	$.114$

* is the power exponent
** is the rate constant
*** is the variance of Δm for the computed slope

Appendix C

Physical and Mechanical Properties
of Rene 41 and TD Nickel

Bibliography

Anders, Fred, J. Jr., et al. "A Dispersion-Strengthened Nickel Alloy."
Metal Progress, 82:88-91 (December 1962).

Blum, B. S. Determination of Causes of Cracking in Welding Age Hardenable
High Temperature Alloys. ASD Technical Report 61-678. Wright-
Patterson AFB, Ohio: Aeronautical Systems Division, November 1961.

Evans, R. M. Joining of Nickel-Base Alloys. DMIC Report 181.
Columbus, Ohio: Defense Metals Information Center, 1962.

Favor, R. J., et al. Design Information on Nickel-Base Alloys for
Aircraft and Missiles. DMIC Report 132. Columbus, Ohio: Defense
Metals Information Center, 1960.

Gorton, C. A., et al. Ultra-Fine High Temperature, High Strength Metallic
Fibers. Technical Report No. ASD-TDR-62-727, Part 1. Wright-
Patterson AFB, Ohio: Aeronautical Systems Division, August 1962.

King, E. J. Mechanical Properties of Rene 41 Sheet Material. Technical
Report. Buffalo, N. Y.: Bell Aerosystems Co., n.d.

Langston, M. E., and Lund, C. H. Physical Properties of Some Nickel-Base
Alloys. DMIC Report 129. Columbus, Ohio: Defense Metals Information
Center, 1960.

Lund, C. H. Current Nickel-Base High-Temperature Alloys. DMIC Memoran-
dum 73. Columbus, Ohio: Defense Metals Informat n Center, 1960.

Machining of Superalloys and Refractory Metals. DMIC Memorandum 134.
Columbus, Ohio: Defense Metals Information Center, 1961.

Manning, Charles R. Jr., et al. An Investigation of a New Nickel Alloy
Strengthened by Dispersed Thoria. NASA TN D-1944. Washington, D. C.:
National Aeronautics and Space Administration, July 1963.

Mitoff, S. P. Electrical Conductivity and Thermodynamic Equilibrium in
Nickel Oxide. Report 61-RL-2606M. Schenectady, N. Y.: General
Electric Research Laboratory, January 1961.

Morris, R. J. "Rene 41...New Higher-Strength Nickel Base-Alloy," Metal Progress, 76:67 (December 1959).

"New Nickel Beats Superalloys Above 2000 F." Materials in Design Engineering, 56:12013 (August 1962).

Popp, H. G. Materials Property Data Compilation. Part I: Rene 41 Sheet and Strip. Cincinnati, Ohio: General Electric Company, 1962.

Starratt, F. Weston. "Dispersion-Strengthened Alloys Become Commercial." Journal of Metals, 14:561-562 (August 1962).

Udimet 41. Advertising brochure. New Hartford, New York: Metals Division, Kelsey-Hayes Company, n.d.

"Ultrafine Oxides Upgrade Metals." Iron Age, 189:73-75 (28 June 1962).

Wahlin, B. M., and Coles, D. R. "How to Make Reliable Seam and Spot Welds in Rene 41." Metal Progress, 80:67 (December 1961).